NASA CR 54830
AGC 8800-74

NASA

N66 28542

ANALYTICAL AND EXPERIMENTAL VIBRATION ANALYSIS

OF THE TURBINE BUCKETS

FOR THE M-1 LIQUID OXYGEN TURBOPUMP

By

L. K. Severud
T. Chinn

Prepared for

National Aeronautics and Space Administration

Contract NAS 3-2555

AEROJET
GENERAL TIRE
GENERAL

AEROJET-GENERAL CORPORATION

SACRAMENTO, CALIFORNIA

Requests for copies of this report should be referred to:

National Aeronautics and Space Administration
Office of Scientific and Technical Information
Attention: AFSS-A
Washington, D. C. 20546

TECHNOLOGY REPORT

ANALYTICAL AND EXPERIMENTAL VIBRATION ANALYSIS
OF THE TURBINE BUCKETS
FOR THE M-1 LIQUID OXYGEN TURBOPUMP

Prepared for

NATIONAL AERONAUTICS AND SPACE ADMINISTRATION

CONTRACT NAS 3-2555

Prepared by:

AEROJET-GENERAL CORPORATION
LIQUID ROCKET OPERATIONS
SACRAMENTO, CALIFORNIA

AUTHOR: L. K. Severud
        T. Chinn

APPROVED: W. E. Watters, Manager
            M-1 Turbopump Project

Technical Management:

NASA LEWIS RESEARCH CENTER
CLEVELAND, OHIO

TECHNICAL MANAGER: W. W. Wilcox

APPROVED: W. W. Wilcox
                    M-1 Project Manager

ABSTRACT

2854 2

The shrouded turbine bucket natural frequencies and associated resonant shaft speeds for the M-1 Liquid Oxygen Turbopump are presented in this report. Both analytical and experimental analysis are discussed and correlated.

Using the experimental findings, the operating range of 3500 rpm to 4000 rpm was investigated for reasonant points. Analysis showed that the first-stage blade package could develop a secondary resonant problem as a result of its second mode of tangential vibration being excited by the second harmonic of the upstream 43 nozzle blade stimulus. No resonant problems are expected for the second-stage blade packages.

TABLE OF CONTENTS

TABLE OF CONTENTS (Continued)

LIST OF TABLES

LIST OF FIGURES

LIST OF FIGURES (Continued)

I.   SUMMARY

The analytical and experimental determination of the natural frequencies of the turbine blades/packages was completed for the first-stage and second-stage rotors of the two stage turbine design of the oxidizer turbopump for the M-1 Engine. The correlation reveals quantitive agreement between measured and predicted frequencies for the range extending up to 10,000 cps. In addition, mode shape measurements provide qualitative identification of the predicted shapes associated with these frequencies.

Using the natural frequency data for the various blade package combinations, the possibility of developing blade operating resonances was studied. Some resonances were found in the operating range. They consisted of the higher harmonics of blade passing stimulus coinciding with higher mode natural frequencies. These resonances are sharp, which means that the stimulus must be very near the natural frequency to excite the blades to any appreciable amplitude of vibration. However, the condition of narrow resonant response does not entirely eliminate resonances as a potential problem.

II.   INTRODUCTION

The purpose of this analysis was to study the possibility of developing resonances of the Model II oxidizer turbine blades packages at various shaft speeds. The natural frequencies of the blades must be known to predict these resonance points. Resonance exits when the fundamental or higher harmonic frequency of the exciting force coincides with a natural frequency of the blade.

Natural frequencies are evaluated analytically by means of a numerical procedure that performs a detailed analysis of a shrouded group of blades. All of the natural frequencies and associated mode shapes (tangential, axial, and torsional) which fall in any specified frequency range can be ascertained.

For purposes of correlation with the analysis, the spectrum of natural frequencies for the first-stage and second-stage turbine rotors was determined experimentally in the range of 50 cps to 10,000 cps. Frequencies and qualitative mode shapes were evaluated for the four-blade and five-blade groups in each rotor stage. The turbine stator was not tested.

III.   VIBRATION ANALYSIS

   ## A.   DESCRIPTION OF THE TURBINE SYSTEM

   ### 1.   Actual Turbine Blade Configuration

   The Model II Oxidizer Turbopump Assembly turbine system consists of: a first-stage rotor blade, P/N 286528; a stator blade, P/N 286545; and a second-stage rotor blade, P/N 286536. The turbine system layout is shown in Figure No. 1.

Nozzle
43 Vanes

Shroud

1st Stage
Turbine
P/N 286531
98 Blades
(4 & 5 Blade package)

Stator P/N 286545
97 Blades
(5 & 6 Blade Package)

Shroud

2nd Stage Turbine
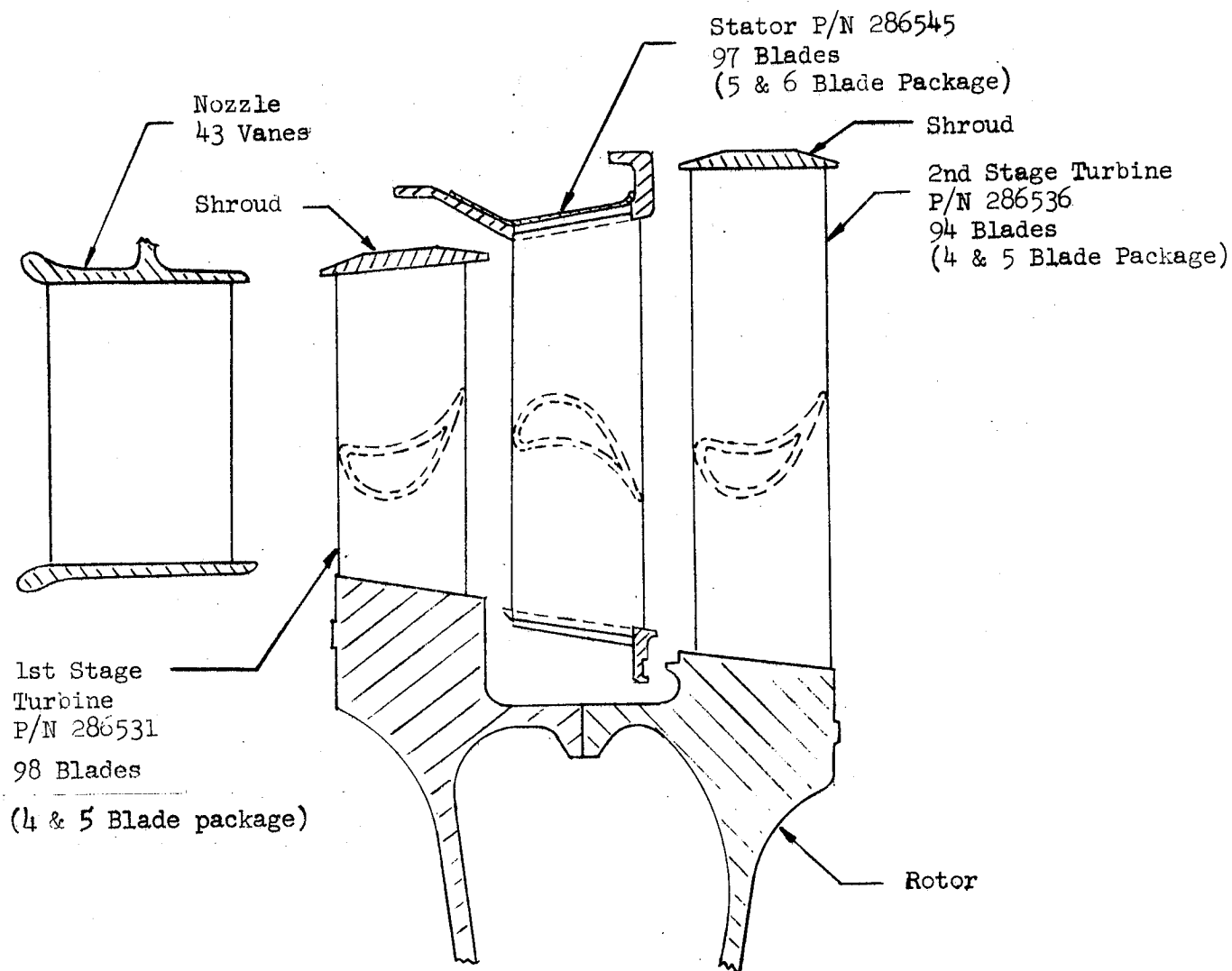P/N 286536
94 Blades
(4 & 5 Blade Package)

Rotor

Figure No. 1

Model II Oxidizer Turbopump Assembly Turbine Blade Set-Up

The Model II Oxidizer Turbopump Assembly first-stage rotor blade consists of 98 blades banded together in groups of four and five blades. The blades, which are made of Inconel 718 material are interconnected by a shroud, which is also made of Inconel 718. A detail of the blade and shroud configuration of the first-stage rotor blade is shown in Figure No. 2. The rotor blades are fixed to the hub and shroud by welding and brazing. Note that the blade section at the hub is reduced at the trailing edge.

The first-stage rotor blade length varies from 3.52-in. at the leading edge to 3.88-in. at the trailing edge. The shroud is canted at an angle of six-degrees, fifteen-minutes. The turbine blade pitch at a mean diameter of 33.00-in. is .997-in. and at the shroud, the pitch is 1.074-in.

The Model II Oxidizer Turbopump Assembly stator blade, consists of 97 blades shrouded together in groups of five and six blades. Because the stator blade vibration analysis will not be reported, a detailed description is omitted from this report.

The Model II Oxidizer Turbopump Assembly second-stage rotor blade (see Figure No. 3) consists of 94 blades banded together by means of a shroud in groups of four and five blades. The blade geometry of the second-stage rotor is identical to the first-stage rotor blade. However, the second-stage shroud is slightly shorter than the first-stage shroud and it is not canted. The blades are fixed at the shroud and hub by means of welding and brazing. Again, a reduction of section properties occurs at the hub.

The second-stage blades are longer than the first-stage blades. They vary in length from 5.5-in. at the leading edge to 5.7-in. at the trailing edge. The blade pitch at the mean diameter of 32.815-in. is 1.016-in. whereas the blade pitch at the shroud is 1.196-in.

2.   Simulated Blade Package for the Vibration Test

A simulated blade package for the first-stage and second-stage rotor was manufactured for the vibration tests. The first-stage rotor, P/N 286529, (Figure No. 4) and the second-stage rotor, P/N 286332, (Figure No. 5) consist of four-blade and five-blade packages banded together by a shroud. The geometry of the blade hub end shroud conforms to the Model II specifications.

The blade fixity at the shroud and hub are the same as in the design of the Model II blades. For the vibration test, the simulated blade package is mounted on a holding fixture (see Figure No. 6) which is then bolted to the MB-C60 electro-dynamic exciter.

B.   LUMPED PARAMETER VIBRATION ANALYSIS

1.   Method of Analysis

Shroud

Blade

3.524

3.884
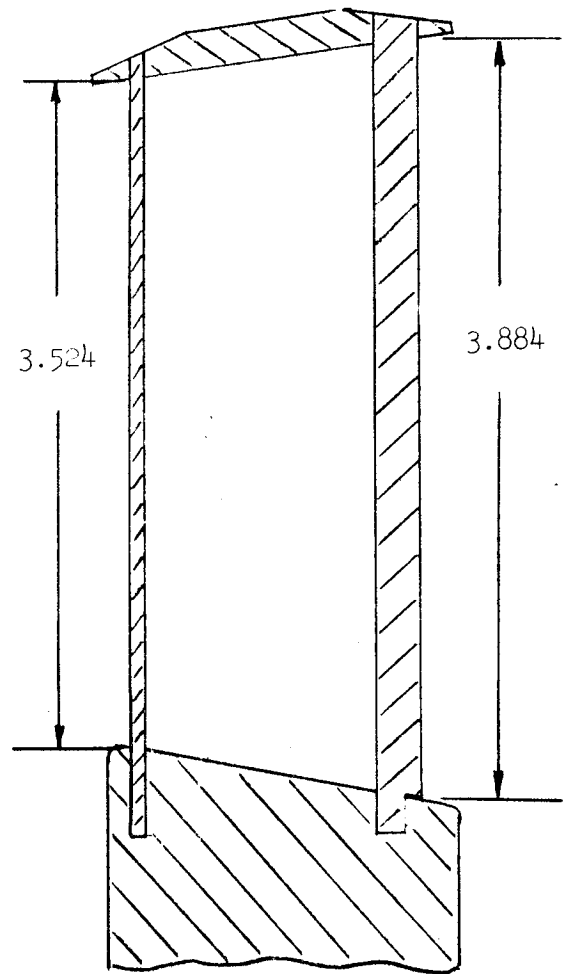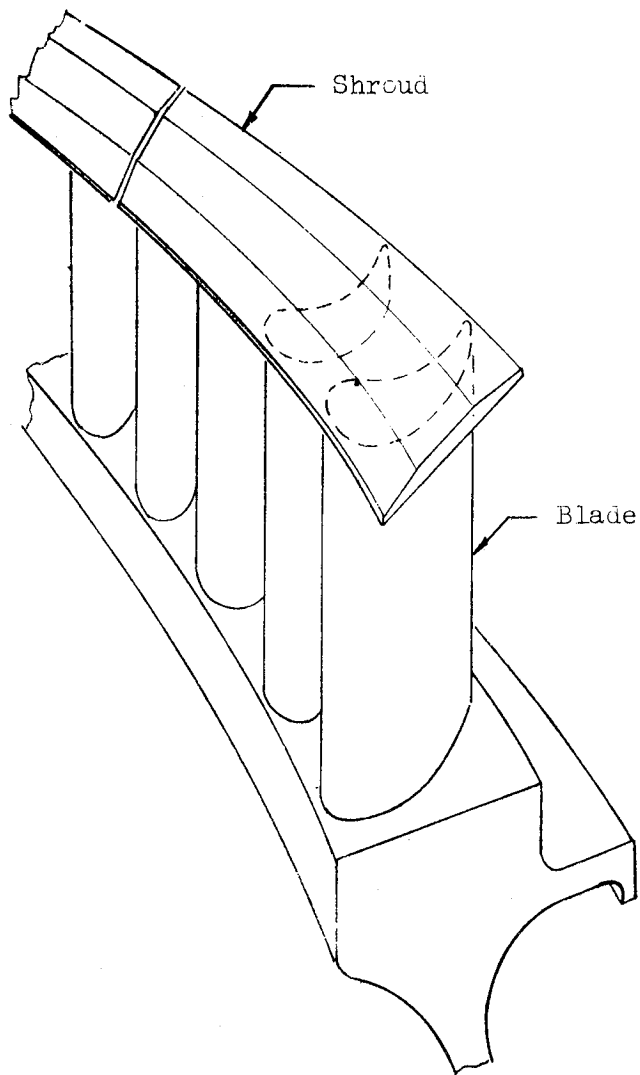
Typical Four-Blade Package

Figure No. 2

First-Stage Turbine Blade, P/N 286531

Shroud

Blade

5.428

5.70
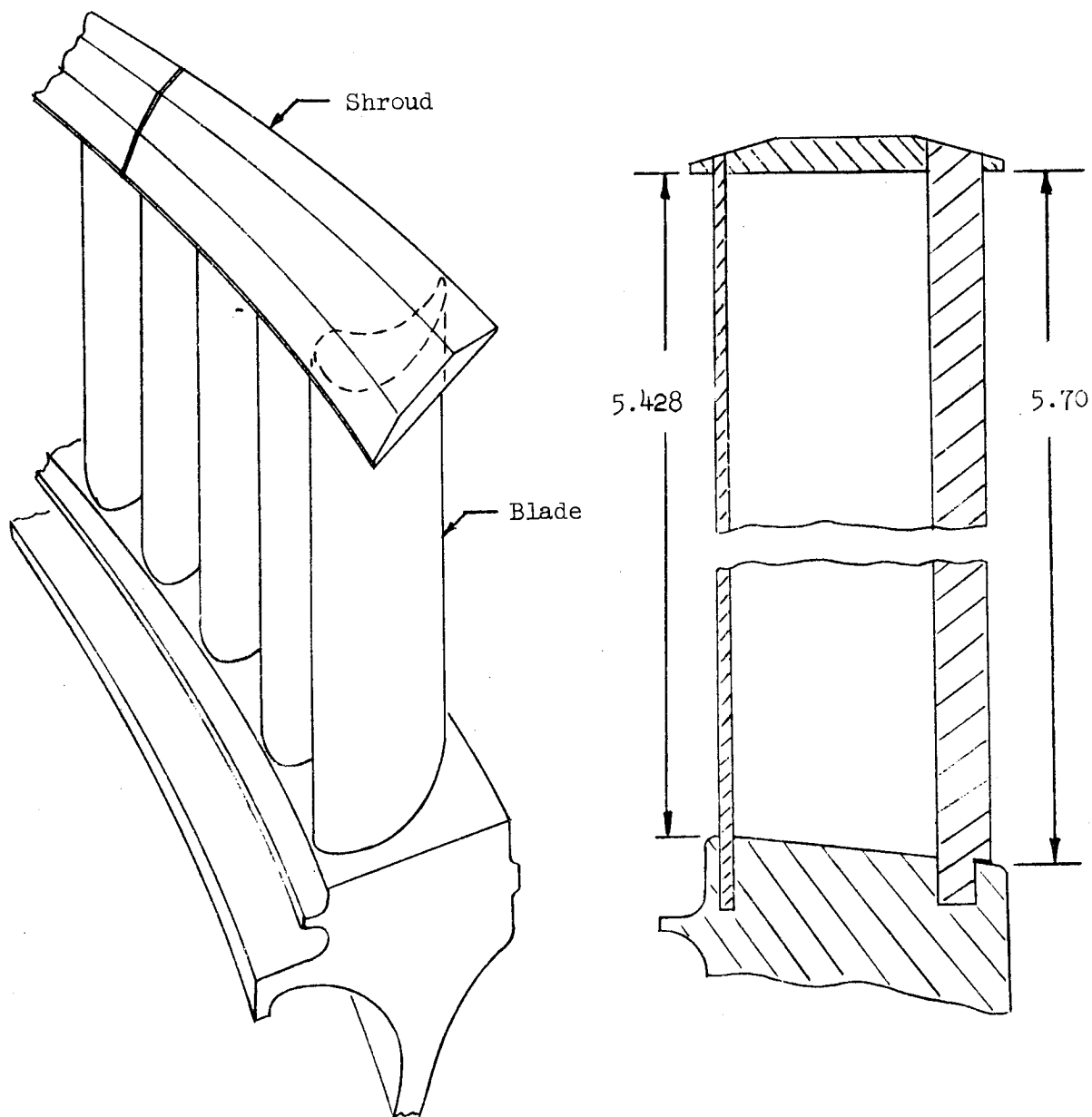
Typical Four-Blade Package

Figure No. 3

Second-Stage Turbine Blade, P/N 286536
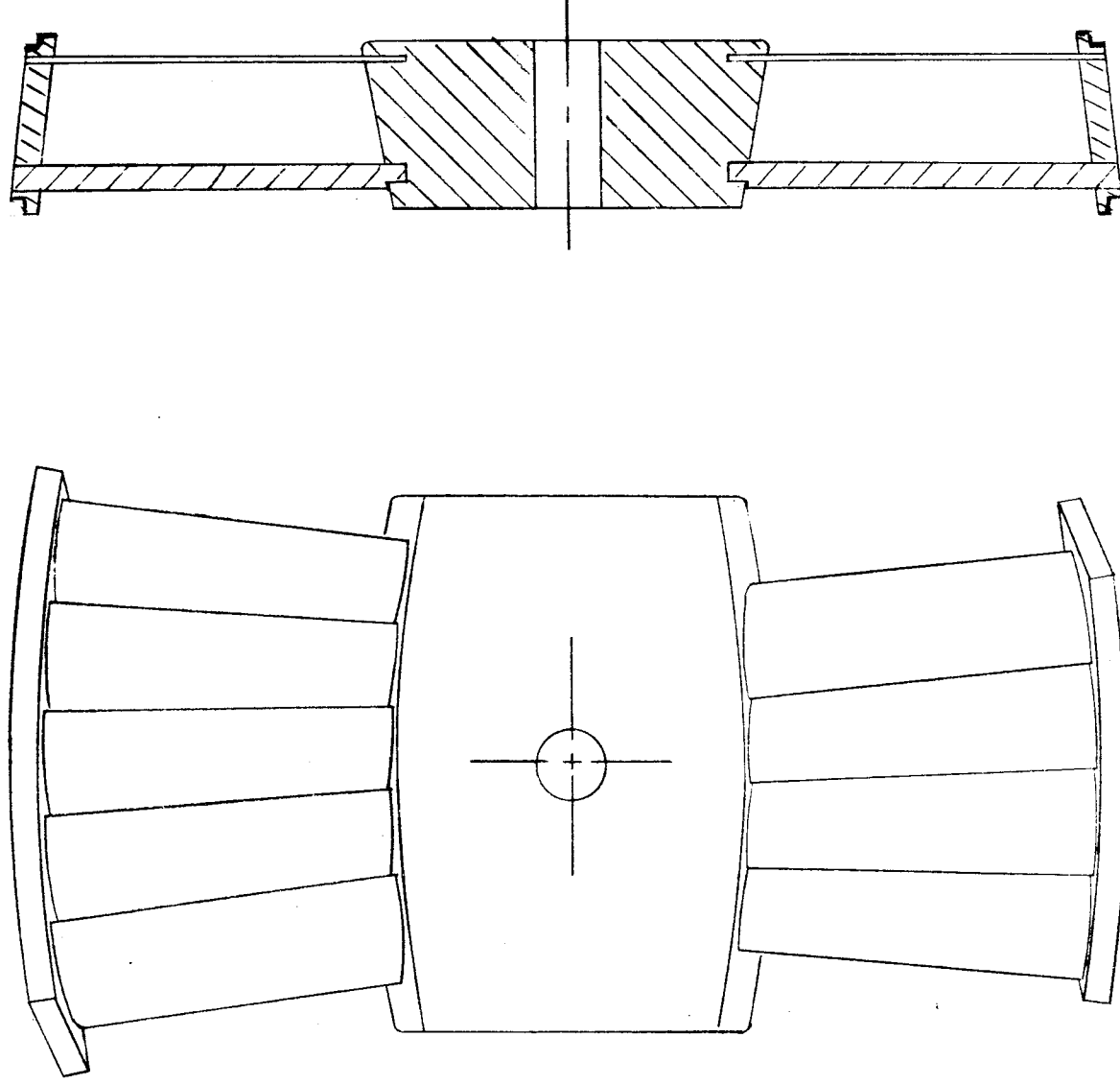
Figure No. 4

First-Stage Simulated Blade Package, P/N 286529

Page 6
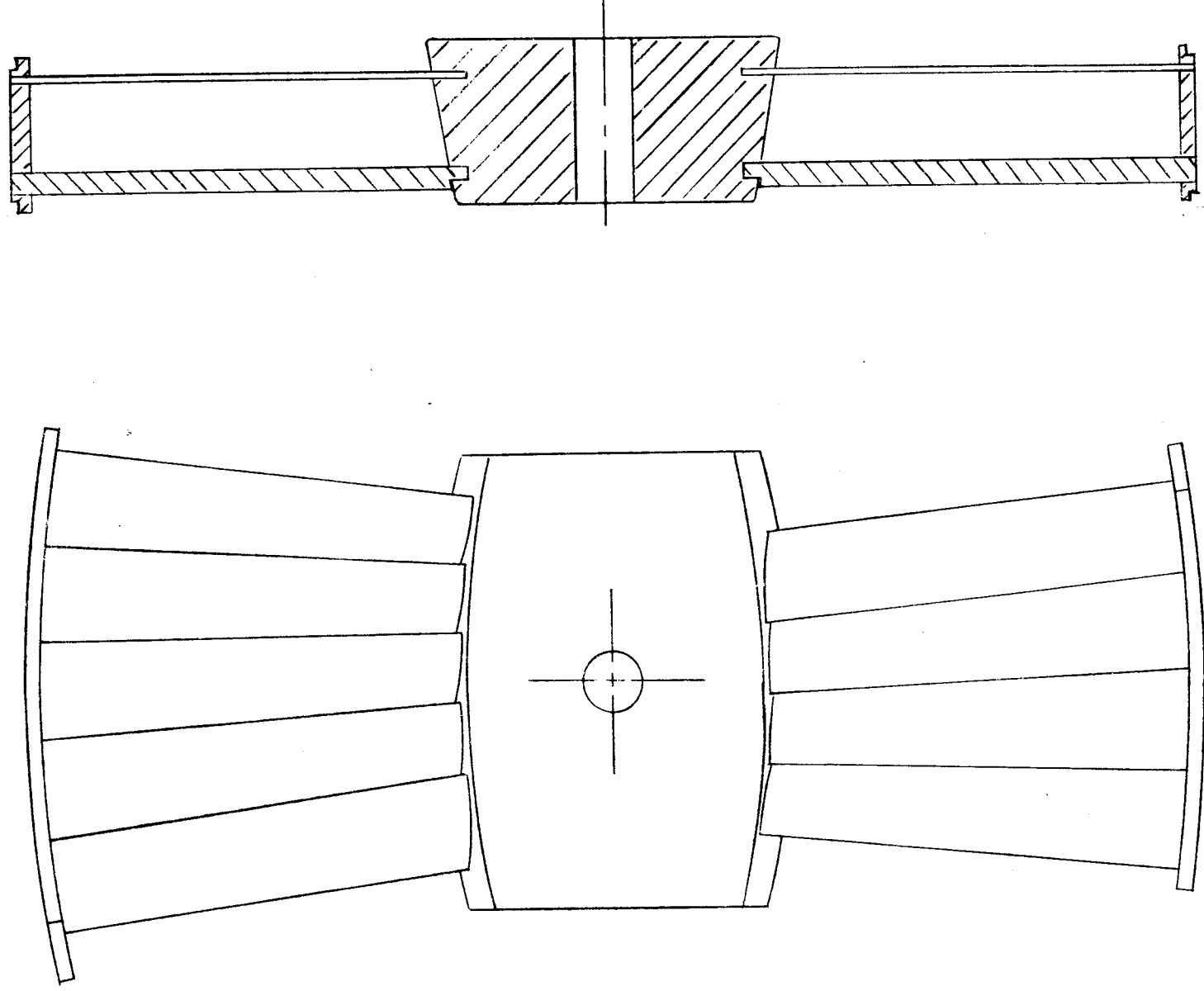
Figure No. 5

Second-Stage Simulated Blade Package, P/N 286532

Simulated Blade Package

Test Stand
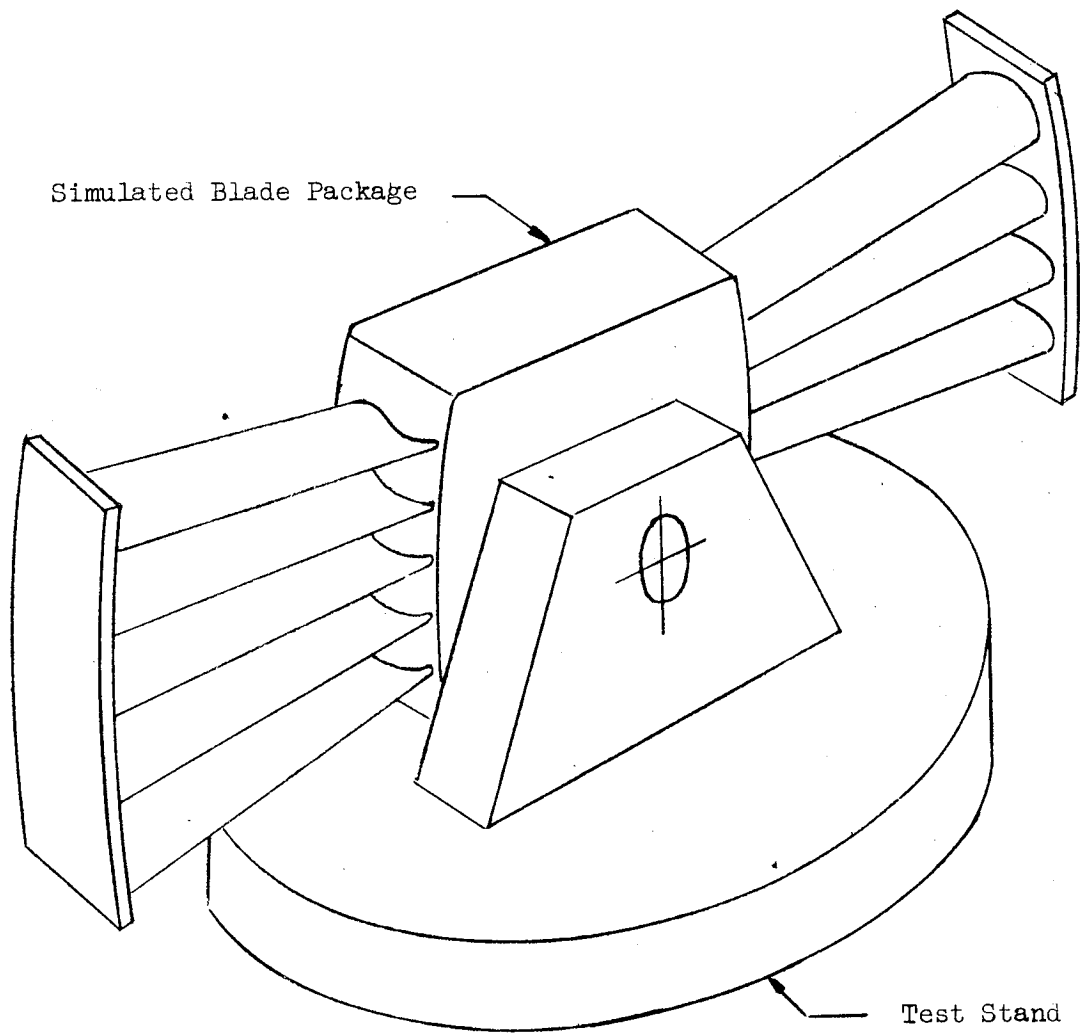
Figure No. 6

Test Set-Up of Simulated Blade Package for Installation on C-60 Exciter

The natural frequencies of the banded turbine blades were predicted utilizing two Aerojet-General Corporation computer programs, which are for in-plane and out-of-plane vibrations of in-plane structures.

a.   Assumptions

The application of these computer analyses for the frequency and mode-shape prediction for the banded group of blades requires the following assumptions:

(1)   The system consists of a series of buckets, elastically jointed at the tip by a shroud.

(2)   The principal axes of inertia of all bucket cross-sections are oriented in the tangential and axial directions, respectively.

(3)   The center of twist of each bucket cross-section coincides with the center of gravity of that cross-section.

(4)   The mass distribution of the buckets can be represented sufficiently as lumped masses.

The lump parameter approach assumes that a mass distribution can be idealized by a system of lumped masses at a discrete point. The structure to be analyzed is defined as a main system with branches. For example, consider the following structures:
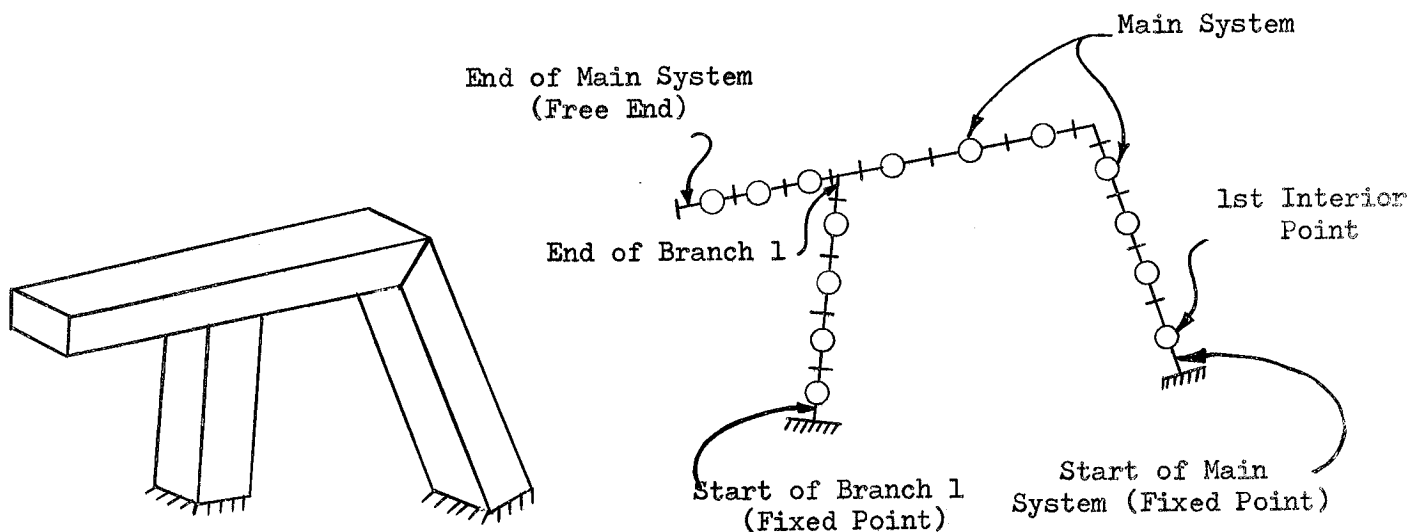
b.   Mathematical Model

The computer program analyzes a system by relating the conditions of state (i.e. Moments, Shear, Axial Forces, Deflections, Rotations, etc.) at the first interior point to the boundary conditions at the start; then in turn, relating the conditions at the second interior point to the first interior point, which then relates the second point to the start. This procedure is continued along the main system until the joint of the first branch is reached. Then, this relating start-to-interior-points technique is used on the branch until the end of Branch 1 is related to its start. Applying the Branch 1 start boundary conditions at the end-to-start relationships, the forces at branch and in terms of its displacements are obtained. This allows the conditions of the main system past the branch to be related to the condition before the branch. The procedure is continued until the end of the main system is related to the last interior point and hence to the start. By utilizing the known boundary conditions at the start and end, the unknown boundary conditions can be evaluated. Then, all the interior conditions can be evaluated by "re-walking" through the main system and branches.

To facilitate this "walking through" technique, transfer matrices are utilized to get conditions of one end in terms of the other end. To illustrate, consider a lumped parameter model broken into bays, a typical bay is shown below:
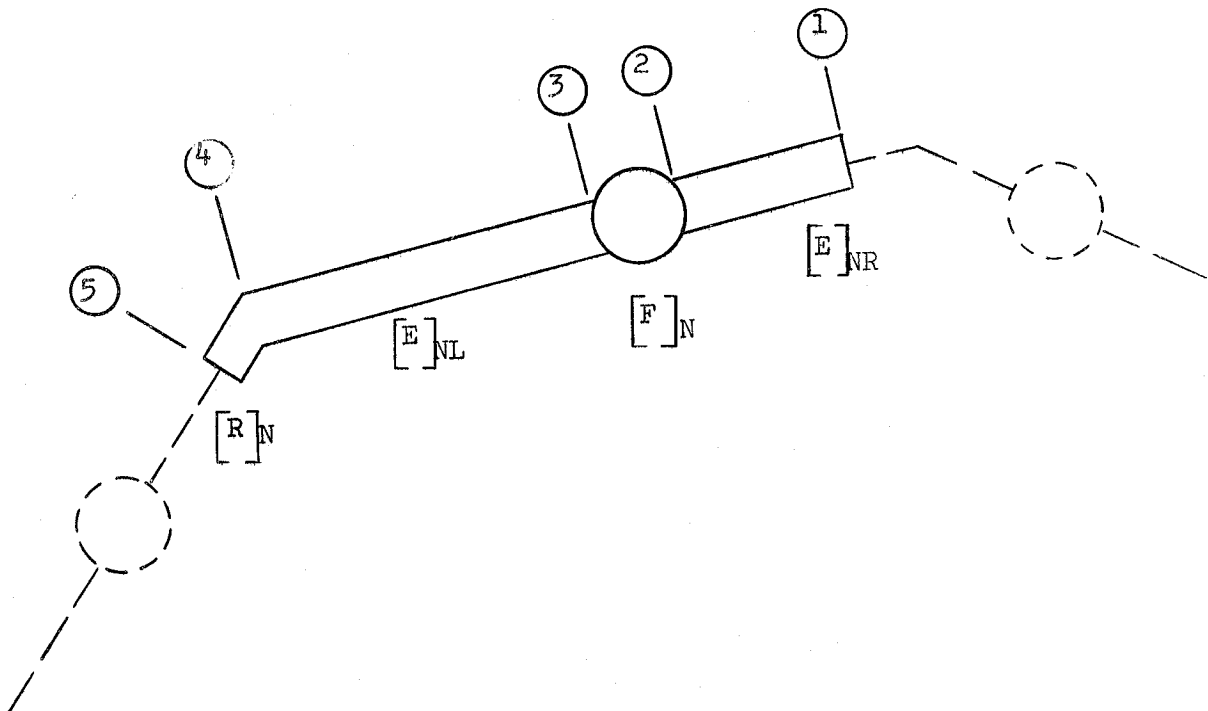
Let $\{\Delta\}_N$ be the state vector as point n. Then, an elasti-
city matrix $[E]$ gets the conditions of state at ② in terms of ① and the applied
loading between ② and ① . The mass matrix $[F]$ relates ③ to ② another elas-
ticity transfer matrix $[E]$ gets conditions at ④ in terms of ③ , and the angle
joint transfer matrix $[R]$ gets ⑤ in terms of ④ . Hence, from the above proce-
dure:

$$\{\Delta\}_② = [E]_{IR} \ \{\Delta\}_① = [E]_{IR} \ \{\Delta\}_{START}$$

$$\{\Delta\}_③ = [F]_1 \ \{\Delta\}_② = [F]_1 \ [E]_{IR} \ \{\Delta\}_{START}$$

$$\{\Delta\}_④ = [E]_{IL} \ \{\Delta\}_③ = [E]_{IL} \ [F]_1 \ [E]_{IR} \ \{\Delta\}_{START}$$

$$\{\Delta\}_⑤ = [R]_1 \ \{\Delta\}_④ = [R]_1 \ [E]_{IL} [F]_1 \ [E]_{IR} \ \{\Delta\}_{START}$$

Thus, it follows that for a multiple bay structure, the start to $[\Delta]_V$ relationship is:

$$\{\Delta\}_V = \left[\prod_{N=1}^{N=V} \left([R]_N \ [E]_{NL} \ [F]_N \ [E]_{NR} \right) \right] \{\Delta\}_{START}$$

After the last bay of the first segment of the main system has been related to the
start, the first branch can be "walked through" to obtain the branch joint transfer
Matrix $[B]$, thus, crossing over the branch, the state vector becomes,

$$\{\Delta\}_{X2} \left[\prod_{N=X1+1}^{N=X2} \left([R]_N \ [E]_{NL} \ [F]_N \ [E]_{NR} \right) \right] [B]_1 \ \{\Delta\}_{XL}$$

Continuing on through to the end of the main system, the final state vector becomes:

$$\{\Delta\}_{END} = \left[\prod_{i=1}^{i=j+1} \left[\prod_{N=X(i-1)+1}^{N=X_i} \left([R]_N \ [E]_{NL} \ [F]_N \ [E]_{NR} \right) \right] [B]_{i-1} \right] \{\Delta\}_{START}$$

Page 11

Where: $[B]_0 = [I]$ unity matrix; $[B]_{i=1}$ For $i > 1$ is as defined in Appendix A.

j = number of branches

The state matrix and the transfer matrix derivations are given in Appendix A for in-plane and out-of-plane loading.

c. Use of Symmetry and Anti-Symmetry Model

When a banded group of blades vibrates in the axial direction, the mode shapes tend to take on either symmetric or anti-symmetric appearance. Thus, the frequencies for the modes can be computed by considering only one-half of a banded group of blades. By using the method of symmetry (i.e., utilizing appropriate boundary conditions at the point of symmetry), the mode shape of the entire banded group can be determined. The above procedure also applies to the blades that behave in an anti-symmetric manner. This procedure was used only in the axial vibration analysis; however, it can also be used for tangential vibration analysis.

A schematic with the boundary conditions for a symmetric and anti-symmetric case is shown below:

$$V = 0 \qquad M = 0$$
$$\phi = 0 \qquad \theta = 0$$
$$Q = 0 \qquad Y = 0$$

Symmetry   Anti-Symmetry
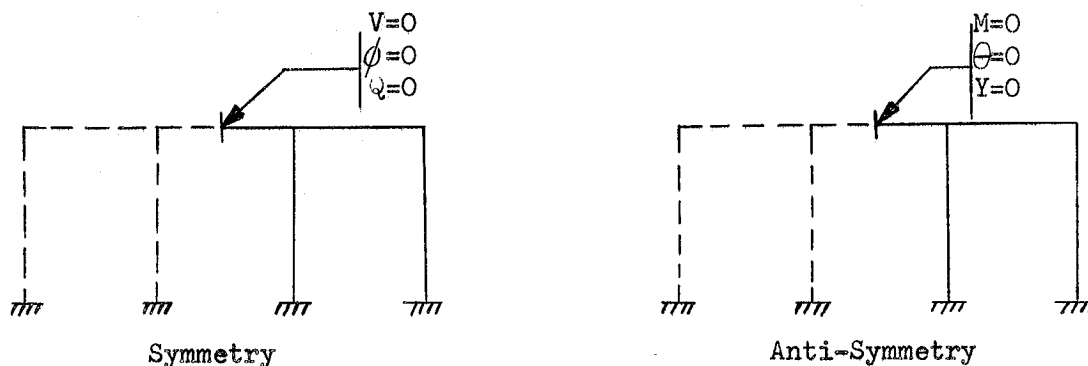
The anti-symmetry analysis yields the frequencies for the odd number modes, while the symmetry method is used to evaluate the even number modes.

The use of the symmetry and anti-symmetry method of analysis for axial vibration is limited to a banded group having an even number of blades. Thus, for the vibration analysis of the first-stage and second-stage rotor blades, only the four-bladed group was determined. However, this method is more accurate than when the total system is considered because only half as many computations are required.

2. Model Representation

A lump parameter model for the Model II Oxidizer Turbopump Assembly turbine bucket blades and shroud attachment are shown in Figure No. 7 for the

Shroud

W_s

L_4 L_3 L_3 L_4

Boundary Condition

L_2 (Typ)

Blade

W_B

L_1

Tangential

Axial
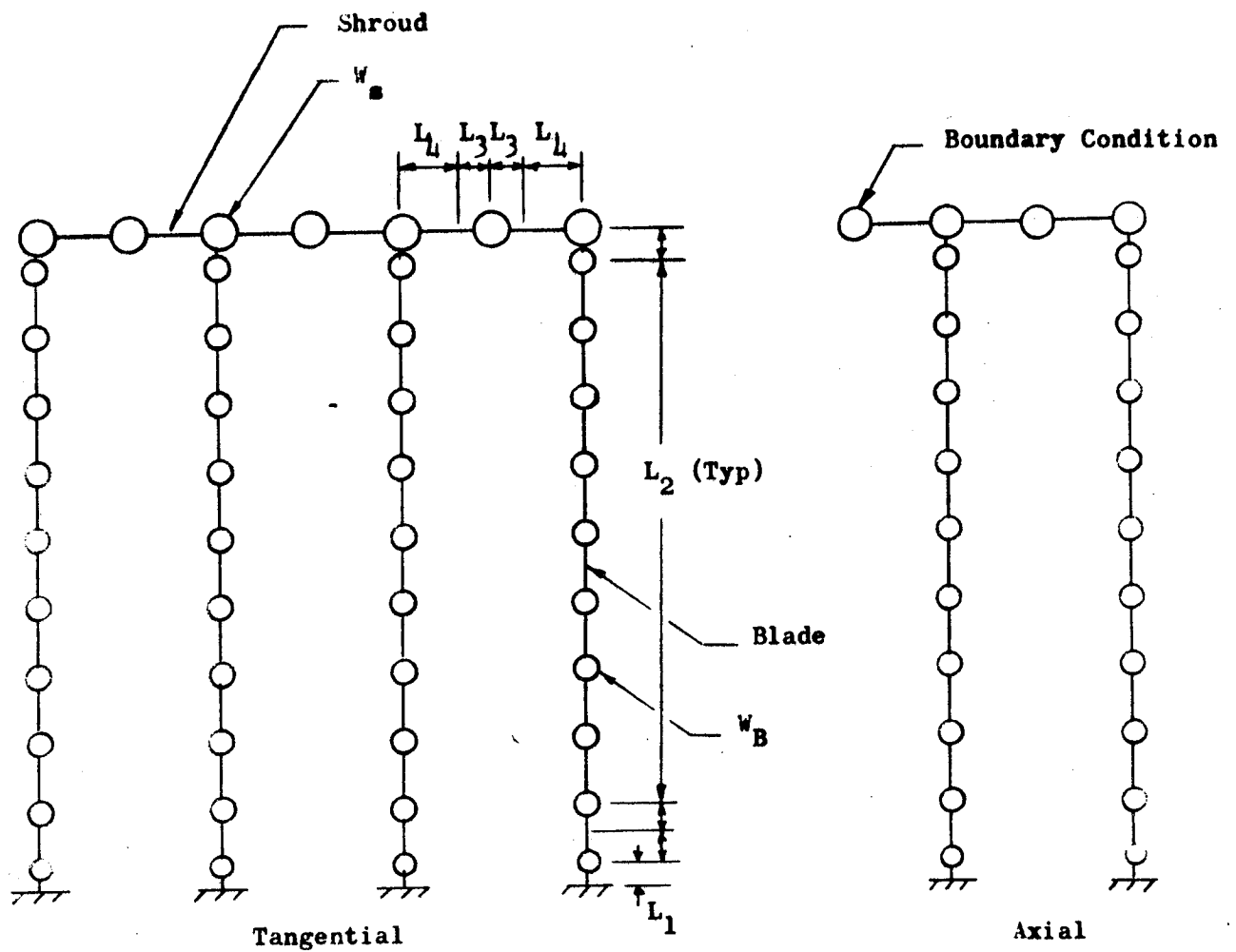
Blade	Blade Properties			Shroud Properties		
	L_1 (in)	L_2 (in)	$W_{B/in}$ (LB$_{/in}$)	L_3(in)	L_4 (in)	$W_{s/in}$ (LB$_{/in}$)
First Stage	.04	.207	.0674	.25	.34	.1043
Second Stage	.04	.315	.0674	.25	.35	.1043

L = bay length

W = weight

Figure No. 7

Lump Parameter Model

Page 13

tangential and axial vibration analysis. This model represents a four-blade package. The model for the axial vibration utilizes the symmetry and anti-symmetry method of approach.

The lump parameters between the first-stage and second-stage blades differs not only in the shroud properties but also in the length of the blades and the shroud pitch. The length of bays and the blade masses for the computer program are tabulated in Figure No. 7 for both the first-stage and second-stage blades.

The turbine bucket section properties for both first-stage and second-stage are identical. The area and moment of inertia of the bucket sections are shown in Table I. The section properties at the bucket fixity to the hub have been reduced slightly to simulate the actual section. In essence, this reduction lessens the bucket stiffness at the hub.

The section properties of the shroud for the first-stage and second-stage blades are shown in Table II. The shroud configuration used in the computer program analysis is the actual geometry of the simulated test blade package. The section properties include the area, moment of inertias, shear deflection constant k, and torsional constant K.

3. Numerical Results

a. Mode Shapes and Frequencies

The mode shapes and frequencies for the Model II Oxidizer Turbopump Assembly first-stage and second-stage rotor blades have been determined by utilizing the matrix transfer technique and the lump parameter models (see Figure No. 7). Further discussion of the tangential, axial, and torsional modes follow.

(1) Tangential Mode

The mode shapes and frequencies for the tangential vibration analysis were predicted for the first-stage and second-stage rotor blades. These are summarized in Table III for the four-blade package and Table IV for the five-blade package.

The results show that between the first and second tangential modes, there is a group of frequencies which are called the fundamental fixed-supported modes. These modes, which are the first, second, and third modes, are characterized by large vibration amplitudes near the bucket pitch line but very little motion at the tips.

The numerical results also indicate that the number of discrete frequencies in the tangential fixed-supported mode group is always one less than the number of buckets banded together. For example, for a four-blade group there are three discrete frequencies. The vibration patterns of the buckets, as observed

Page 14

TABLE I

TURBINE BLADE SECTION PROPERTIES
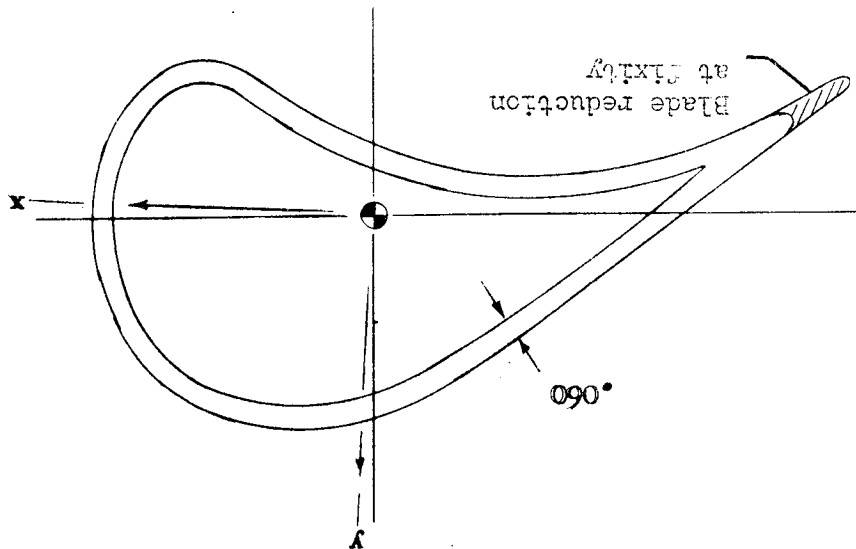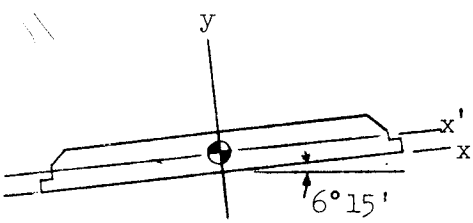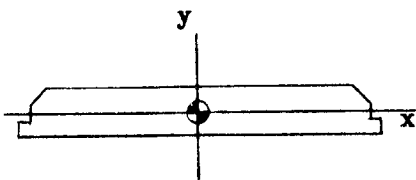
	First-Stage Rotor		Second-Stage Rotor	
		@ Fixity		@ Fixity
Area, in.^{2}	.241	.230	.241	.230
I_{xx}, in.^{4}	.0136	.0128	.0136	.0128
I_{yy}, in.^{4}	.0592	.0496	.0592	.0496
$C_{tang} = \dfrac{k_t}{A}$, $\dfrac{1}{in.^2}$	6.68	7.0	6.68	7.0
$C_{axial} = \dfrac{k_a}{A}$, $\dfrac{1}{in.^2}$	4.90	5.13	4.90	5.13
K (Torsional constant)	.0205		.0205	
Length, in.	3.8		5.8	

C = shear deflection coefficient

K = shear deflection constant

TABLE II

FIRST-STAGE AND SECOND-STAGE SHROUD PROPERTIES

A	$.298$ in.^{2}	$.285$ in.^{2}
$I_{x'x'}$	$.00166$ in.^{4}	$.000864$ in.^{4}
I_{yy}	$.0636$ in.^{4}	$.05585$ in.^{4}
$\bar{y}$	$.0861$ in.	$.087$ in.
$C_{tang} = k_t/A$	$2.01/in.^2$	$5.01/in.^2$
$C_{axial} = k_a/A$	$4.63/in.^2$	$4.80/in.^2$
K (Torsional constant)	$.00589$	$.00589$

C = shear deflection coefficient
k = shear deflection constant

TABLE III

CALCULATED TANGENTIAL AND AXIAL NATURAL FREQUENCIES OF FIRST-STAGE TURBINE
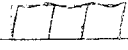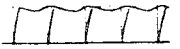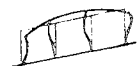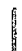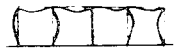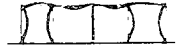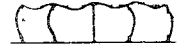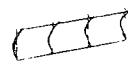
Tangential Mode	Axial Mode	Four-Bucket Group				Five-Bucket Group	
		Tangential	Mode Shape	Axial	Mode Shape	Tangential	Mode Shape
First Cantilever		1471	⌐⌐⌐⌐			1433	⌐⌐⌐⌐⌐
	First Axial Group			2099			
				2409			
				4632			
				4840			
First Fixed-Supported Group		6514				6460	
		6940				6784	
		7082				6914	
						7070	
	Second Cantilever			6969			
Second Cantilever		7979					

TABLE IV

CALCULATED TANGENTIAL AND AXIAL NATURAL FREQUENCIES OF SECOND-STAGE TURBINE

Tangential Mode	Axial Mode	Four-Bucket Group				Five-Bucket Group	
		Tangential	Mode Shape	Axial	Mode Shape	Tangential	Mode Shape
First Cantilever		725	(sketch)			733	(sketch)
	First Axial Group			1086	(sketch)		
				1525	(sketch)		
First Fixed-Supported Group		2520	(sketch)			3510	(sketch)
		2910	(sketch)			3711	(sketch)
		3005	(sketch)			4110	(sketch)
						4310	(sketch)
Second Cantilever		3820	(sketch)				
	First Axial Group			4157	(sketch)		
				4257	(sketch)		
	Second Cantilever			5192	(sketch)		

from the mode shapes (see Tables III and IV) take on "odd" or "even" symmetry appearance depending upon whether corresponding buckets in each half of the group are in-phase or out-of-phase.

(2) Axial Mode

The mode shapes and frequencies for the axial vibration analysis were predicted by using the lump parameter model shown in Figure No. 7. This model utilizes boundary conditions consistent with the symmetric and anti-symmetric modes. The numerical results of the frequencies for the axial vibration of the first-stage and second-stage rotor blades as well as their respective mode shapes are shown in Table IV for the four-blade package.

The first axial group modes are characterized by the progressive pattern of nodes in the shroud band. There are no nodes along the bucket length. In the lowest or first mode, there are no nodes along the shroud band. All of the buckets in the first axial group vibrate in the axial direction and all of their motions are in phase. The second axial mode has one node along the band, the third has two nodes, and so forth. The highest frequency mode always has nodes in the shroud between each bucket in the banded group and thus, the number of nodes along the band is equal to one less than the number of buckets banded together. Therefore, the total number of modes in this axial group is always equal to the number of buckets banded together.

(3) Torsional Mode

For shrouded blades pure torsional modes do not exist. Moreover, the coupled torsional-bending natural frequencies are as predicted for the axial modes of vibration.

C. VIBRATION TESTS OF FIRST AND SECOND STAGE TURBINE ROTOR BLADES

1. Test Set-Up and Procedure

The vibration tests utilizes the simulated blade package (see Section III, A) to determine the various resonant frequencies and corresponding mode shapes. The first-stage rotor, P/N 286529, and second-stage rotor, P/N 286532, each in turn, was mounted in a holding fixture and bolted to the MB-C60 electro-dynamics exciter (see Figure No. 6). The simulated blade packages were excited in both the axial and tangential directions from 100 cps to 9000 cps.

The resonant frequencies were determined by the phase change between the accelerometer output and the excitation input as observed on an oscillo-scope. An Endevco accelerometer was used to pick up the output signal on the blades.

The nodal patterns of the banded blade were determined by using the salt pattern technique and the damping-undamping technique.

Page 19

2. Test Results

The mode shapes and resonant frequencies from the vibration tests of the first-stage and second-stage turbine blades are summarized in Tables V and VI. For the tangential modes, the first cantilever, first fixed-supported, and second cantilever modes were obtained for the first-stage and second-stage turbine blades. For the axial modes, only the first axial group was measured from the vibration test.

The frequency values in the first fixed-supported group for both turbine blades were quite close together, whereas in the first axial group, the frequency varied widely, yet they are lower than the first fixed-supported group.

The test results also indicated that the frequencies of the four-blade and five-blade packages in the higher modes are similar with the exception that the five-blade package has one more mode than the four-blade package. Thus, use of the four-blade package data is sufficient for evaluation of resonance.

3. Correlation of Test Frequencies with Analytical Predictions

A comparison between calculated and observed frequencies of banded bucket groups is presented in Table VII for the four-blade and five-blade banded groups of the first-stage and second-stage rotor blades.

In the tangential mode, comparison of frequencies is given for the four-blade and five-blade groups, whereas in the axial direction only frequencies from the four-blade banded group were measured. The results, which are very encouraging, indicate that fairly accurate predictions of resonance conditions can be accomplished through the use of these digital computer programs. Therefore, these computer programs can aid in the future design efforts of banded buckets.

The discrepancies between the test values and the computer predictions in the higher modes could largely be the result of the blade orientation; that is, the shroud is actually of such a nature as to couple, although weakly, the tangential and axial modes of vibration. Also, the treatment of the shroud stiffness and "effective" length becomes more significant in the prediction of blade frequencies in the higher harmonics. In the analytical prediction analyses, the effective length influence was accounted for by distributing the shroud stiffness as shown in Figure No. 8.

D. RESONANT FREQUENCY DETERMINATION

1. Excitation Frequencies

a. Description of Primary Stimulus for Each Stage

The natural frequencies of the turbine blades are excited by the action of periodic stimulus which, in this case, is a gas flowing through a

TABLE V

OBSERVED TANGENTIAL AND AXIAL NATURAL FREQUENCIES OF FIRST-STAGE TURBINE
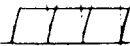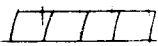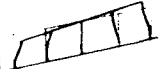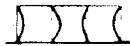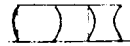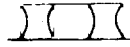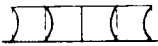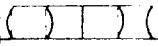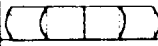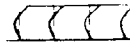
Tangential Mode	Axial Mode	Four-Bucket Group				Five-Bucket Group			
		Tangential	Mode Shape	Axial	Mode Shape	Tangential	Mode Shape	Axial	Mode Shape
First Cantilever		1220	[mode shape sketch]			1335	[mode shape sketch]		
	First Axial Group			1480	[mode shape sketch]			1460	[mode shape sketch]
				1900	[mode shape sketch]			1960	[mode shape sketch]
				4550	[mode shape sketch]			6590	[mode shape sketch]
				6510	[mode shape sketch]				
First Fixed-Supported Group		6635	[mode shape sketch]			5560	[mode shape sketch]		
		6820	[mode shape sketch]			6220	[mode shape sketch]		
		6920	[mode shape sketch]			6410	[mode shape sketch]		
						6655	[mode shape sketch]		
Second Cantilever		7005	[mode shape sketch]			7000	[mode shape sketch]		
	First Axial Group			6969				7980	[mode shape sketch]
								> 9000	[mode shape sketch]

TABLE VI

OBSERVED TANGENTIAL AND AXIAL NATURAL FREQUENCIES OF SECOND-STAGE TURBINE

Tangential Mode	Axial Mode	Four-Blade Package				Five-Blade Package			
		Tangential	Mode Shape	Axial	Mode Shape	Tangential	Mode Shape	Axial	Mode Shape
First Cantilever		725	(sketch)			800	(sketch)		
	First Axial Group			975	(sketch)			960	(sketch)
				1250	(sketch)			1150	(sketch)
				2910	(sketch)			2920	(sketch)
First Fixed-Supported Group		2520	(sketch)			2510	(sketch)		
		2910	(sketch)			2910	(sketch)		
		3005	(sketch)			2950	(sketch)		
						3100	(sketch)		
First Cantilever		3820	(sketch)			3960			
	First Axial Group			5050	(sketch)			5100	(sketch)
								8300	(sketch)

TABLE VII

COMPARISON OF OBSERVED AND CALCULATED TANGENTIAL AND AXIAL NATURAL FREQUENCIES OF FIRST-STAGE AND SECOND-STAGE TURBINE BLADE

	Mode	First-Stage Turbine Blade				Second-Stage Turbine Blade			
		Four-Blade		Five-Blade		Four-Blade		Five-Blade	
		Observed	Calculated	Observed	Calculated	Observed	Calculated	Observed	Calculated
Tangential	First Cantilever	1220	1471	1335	1433	725	722	800	733
	↑ First Fixed-Supported Group ↓	6635	6514	5560	6460	2520	3337	2510	3510
		6820	6940	6220	6784	2910	3541	2910	3711
		6920	7082	6410	6914	3005	3671	2950	4110
				6655	7070			3100	4310
	Second Cantilever	7005	7979	8000		3820	4371	3960	
Axial	↑ First Axial Group ↓	1480	2099	1460		975	1086	960	
		1900	2409	1960		1250	1525	1150	
		4550	4632	6590		2910	4157	2920	
		6540	4840	7980		5050	4257	5100	
				> 9000				8330	

Blade Pitch

Turbine Blade

Shroud

EI

Shroud Stiffness

Shroud Stiffness Across Blade -
Taken as 10 Times
EI of Shroud

Actual EI for Shroud Cross-Section (See Table II)
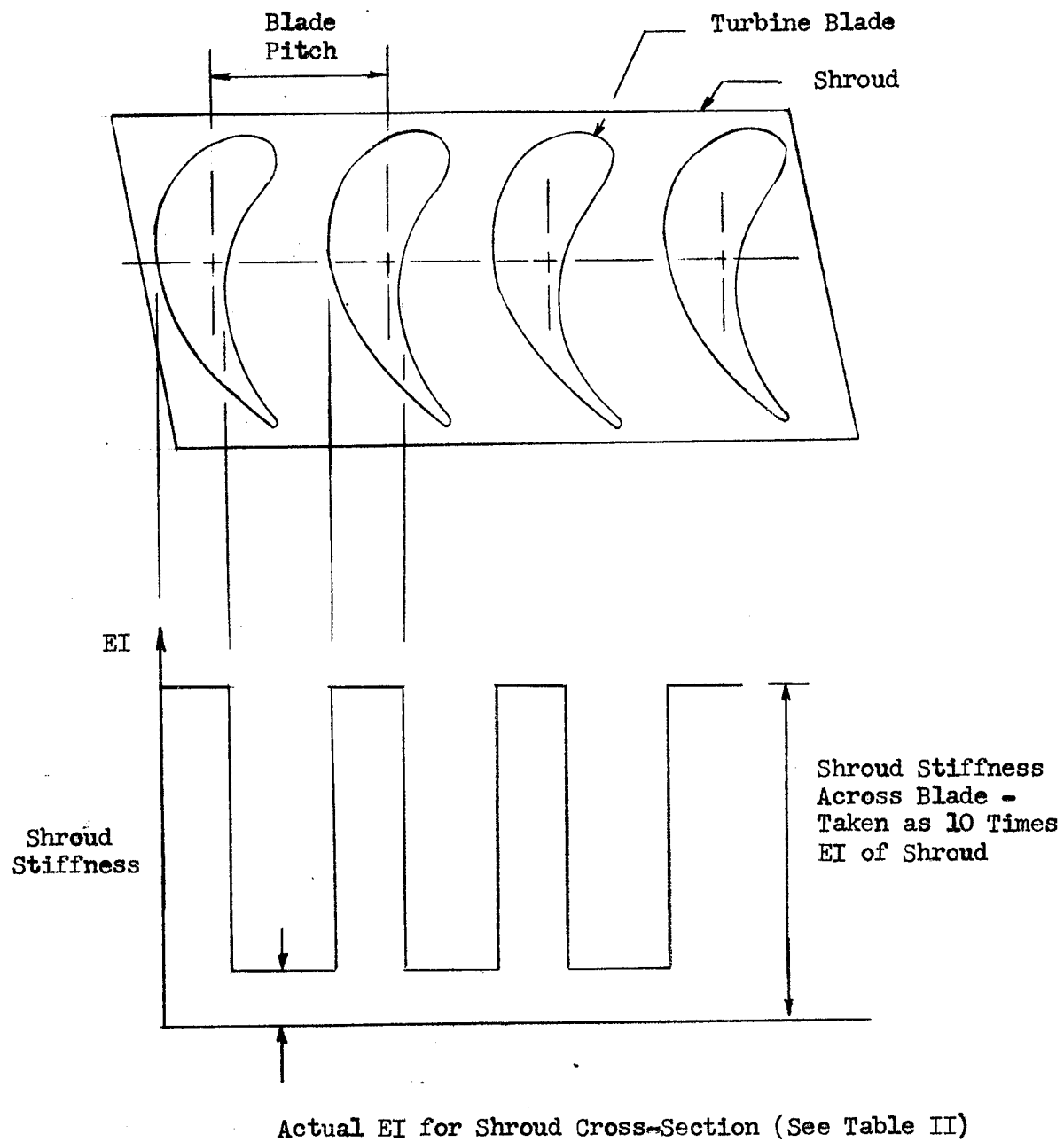
Figure No. 8

Effective Shroud Length for Blade Frequency Predictions

group of nozzles. The stimulus has a period of time equal to the time required for the bucket to travel a distance of one nozzle pitch. Because the stimulus is non-sinusoidal, it can also excite the buckets at frequencies that are multiples of the frequency of passing nozzles.

The frequency of the stimulus may be calculated by

$$\text{Frequency} = \frac{n\,N\Omega}{60}, \text{ cps}$$

where: n = the harmonic

N = number of nozzle per 360 degrees

Ω = shaft speed, rpm

Now, by making a plot of frequency, ω, (cps), versus shaft speed, (rpm), a series of lines representing the frequencies of the stimulus for each harmonic can be drawn, and the slope of these lines is defined as:

$$\text{Slope} = \frac{\text{Freq of Stimulus}}{\text{Shaft Speed}} = \frac{n\,N\left(\frac{\Omega}{60}\right)}{\Omega} = \frac{n\,N}{60}$$

The primary stimulus for the first-stage turbine blades is the result of gas flowing from the 43 turbine nozzle blades. The second-stage turbine blades can be excited by the actions of both the 97 stator blades, which is the primary stimulus, and the 43 nozzle blades (see Figure No. 1).

Plots of the stimulus for the first-stage and second-stage turbine blades are shown in Figures No. 9 and No. 10. Resonant points of the turbine blades (i.e., the point in which the natural frequency coincides with the frequency of the stimulus) are determined by the intersection of the horizontal lines representing the natural frequency of the blades with the stimulus lines. These maps represent "critical speed" plots for the turbine blades. The horizontal lines would become curved lines if centrifugal stiffening of the blades is significant; however, this effect was determined and found to be negligible.

2.   Tangential and Axial Mode Resonance Points

Critical speed plots for the first-stage and second-stage turbine rotor blades are given in Figures No. 9 and No. 10. Because the operating range of the shaft speed is 3500 rpm to 4000 rpm, only the resonance points within the operating band are of interest. It should be noted that for each case, the stimulus frequency curves are for the first three harmonics ($n = 1,2,3$). The amplitudes for the higher harmonics should be very small and can be considered negligible. The turbine blade natural frequencies for the tangential and axial modes are the measured values (see Tables VI and VII) of both the four-blade and five-blade groups. The measured

Page 25
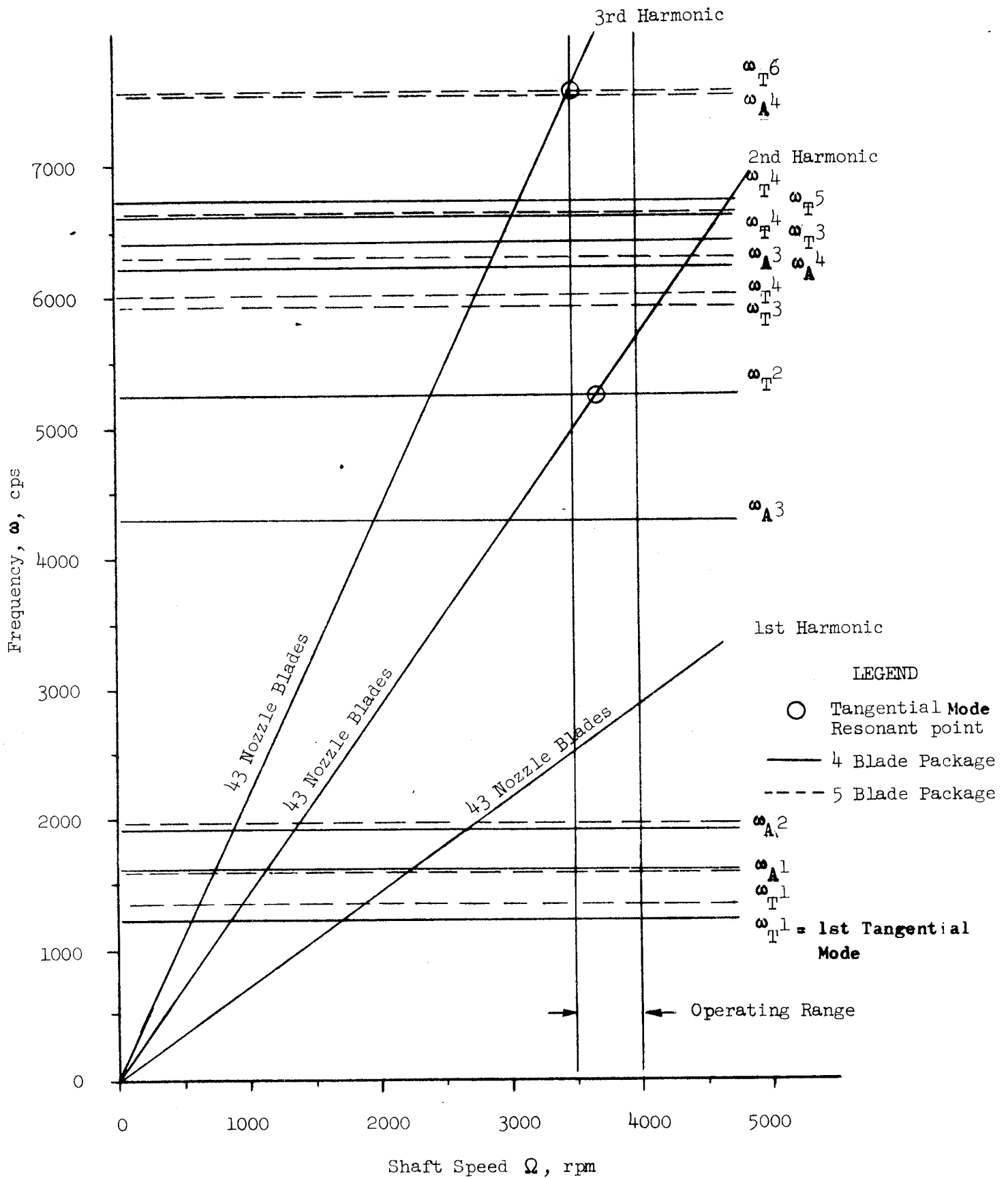
Figure No. 9

Critical Speed Plot at Operating Temperature and Speed,
First-Stage Turbine Blade

Page 26
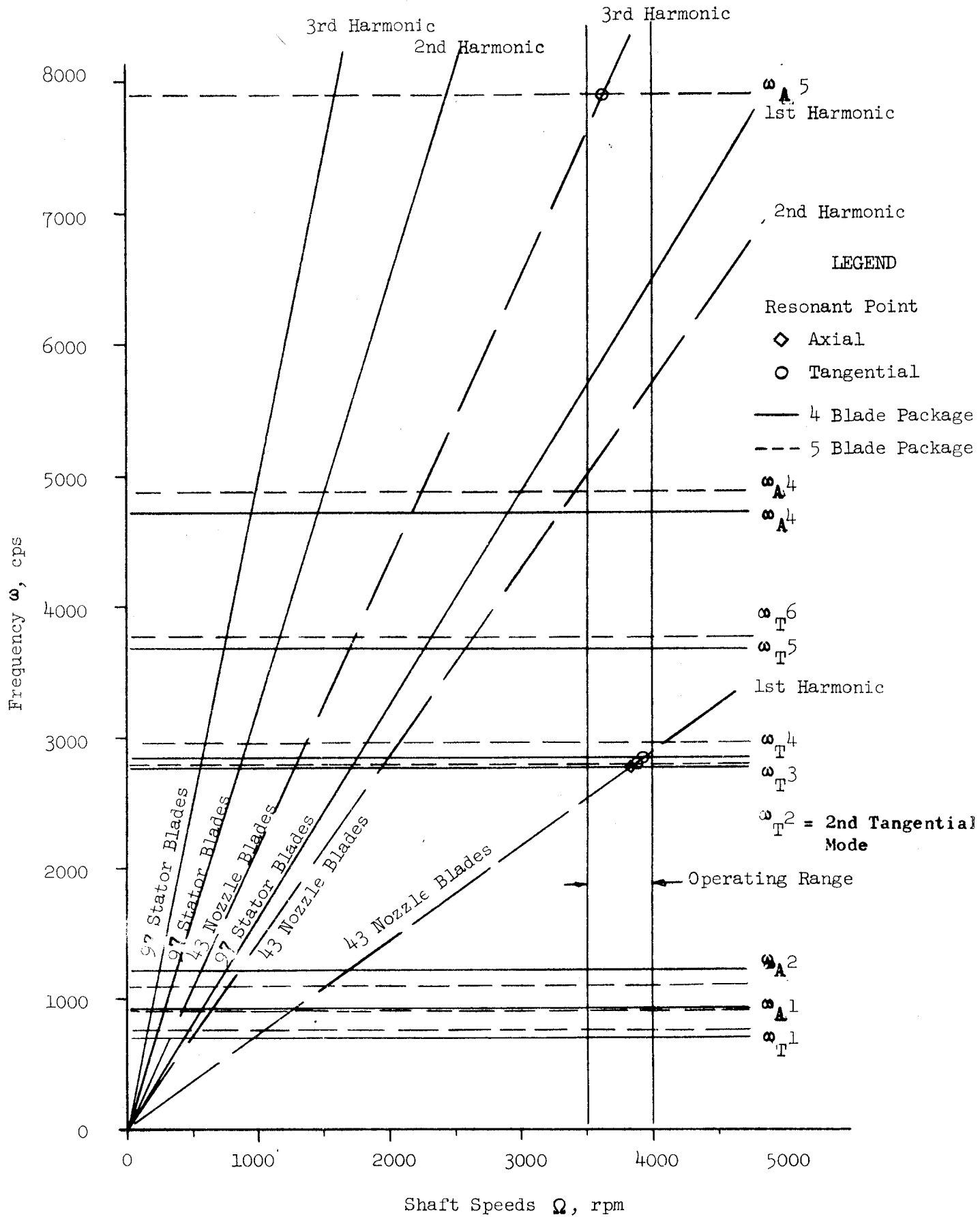
Figure No. 10

Critical Speed Plot at Operating Temperature and Speed,
Second-Stage Turbine Blade

frequencies have been corrected to the operating condition by the ratio of the elastic modulus at operating temperature. Thus, at a temperature of 1100°F, the frequencies are corrected by (.945) x room temperature frequency.

For the first-stage turbine blades, the critical speed plot (see Figure No. 9) indicates that the second harmonic of the exciting force provided by the 43 nozzle blades could theoretically excite the second tangential mode of vibration. The natural frequency for this case is 5270 cps, which corresponds to the first mode in the fixed-supported group.

The critical speed plot of the second-stage turbine blade (Figure No. 10) indicates several resonance points within the operating range, particularly the first harmonic of the secondary stimulus from 43 nozzle blades. The primary stimulus is provided by the 97 reversing blades. The first harmonic of the exciting force provided by the nozzle blades could theoretically excite the first fixed-supported group of the tangential modes and the third mode of the axial vibrations in the five-blade package as well as the similar modes of vibration in the four-blade package. At a higher frequency, the third harmonic of the exciting force from the 43 nozzles could excite the fifth mode (7900 cps) of the axial modes of vibration in the five-blade package. These higher modes of possible resonance are not considered critical because they are more difficult to excite and the exciting stimulus magnitude decreases rapidly with the higher harmonics of the forcing frequency.

3.   Operating Speed Range Potential Vibration Problems

The operating range of the Model II Oxidizer Turbopump Assembly turbine blade is between 3500 rpm and 4000 rpm. Within this operating range, several resonant points occur, particularly with the second-stage turbine blade. However, the excitation force of the second-stage blade has been provided mostly from the 43 nozzle blades which, in this case, is not the primary stimulus. Therefore, the excitation force is not very powerful and hence, a resonance problem is not expected.

For the first-stage turbine, the resonant points within the operating range consist of the second and third harmonic of nozzle passing stimulus exciting the second and sixth modes of tangential vibration. As no fundamental modes have resonant points in the operating range, the turbine blades can operate within the range without any significant resonant problems. If a problem does occur, it probably will be associated with the second mode resonant point excited by the second harmonic of nozzle passing stimulus.

IV.   CONCLUSIONS

The analytical and experimental determination of the natural frequencies of the first-stage and second-stage turbine blades of the Model II Oxidizer Turbopump Assembly has been fully evaluated. The results from the vibration tests of a

simulated blade package, as compared with the analytical solution, demonstrate that the natural frequencies from a shrouded group of blades can be predicted quite well by the technique presented herein.

Discrepancies between the predicted and test data could possibly be the result of the principal bending axis of the blade package not being in the same plane as that of the shroud. For simplicity, in the computer solution, the principal bending direction for both the blade and shroud is taken to lie in the same plane.

Good correlations were obtained in the lower frequencies for both the first-stage and second-stage turbine blades. For the higher modes, natural frequencies of axial vibration predictions tend to be somewhat higher than the test results.

The resonance points of the turbine blades using test results were investigated in the operating range of 3500 rpm to 4000 rpm. For the first-stage blade package, a resonance problem might occur because of the second mode of tangential vibration being excited by the second harmonic of the 43 nozzle blade stimulus. Moreover, this is not considered to be a primary resonant problem as it is not definite that sufficient excitation will occur. No resonant problems are expected for the second-stage blade packages.

BIBLIOGRAPHY

1. Severud, L. K. and Richardson, J. C., User's Manual for Computer Job No. 14051, Vibration and/or Static Structural Analysis of In-Plane Loading of In-Plane Structures with Branches, Aerojet-General Corporation, 15 May 1964

2. Severud, L. K. and Richardson, J. C., User's Manual for Computer Job No. 14055, Vibration and/or Static Structural Analysis of Out-of-Plane Loading of In-Plane Structures with Branches, Aerojet-General Corporation, 18 May 1964

3. Aerojet-General Memorandum No. 9745:956, L. K. Severud to R. Beer, dated 19 October 1964, subject: Vibration Analysis of the M-1, Mod II Oxidizer Turbine Blades

4. Aerojet-General Memorandum No. 9647:3.6-253, V. Drury, dated 29 July 1965, subject: M-1, Mod II, First and Second Stage Turbine Rotor Blades Vibration Test

APPENDICES

APPENDIX A

NOMENCLATURE

A	=	Area, in^2
C	=	Shear deflection coefficient, $1/\text{in}^2$
G	=	Modulus of Rigidity, lb/in^2
g	=	Acceleration of gravity, $386 \ \text{in}/\text{sec}^2$
I	=	Moment of Inertia, in^4
J	=	Rotary inertia constant, $9\text{lbs-sec}^2\text{-in.}$
K	=	Torsional constant
k	=	Shear deflection coefficient
L	=	Length of bay element, in.
M	=	Bending moment, in-lbs
Q	=	Torque, in-lbs
T	=	Axial force, lbs
u	=	Displacement perpendicular to axis of bay element, in.
V	=	Shear force, lbs
y	=	Displacement parallel to axis of bay element, in.
W	=	Weight of bay element, lbs
$\propto$	=	Pitch angle between bay elements, degrees
ϕ	=	Rotation, radians
$\ominus$	=	Torsional Rotation of axis of bay element, radians
ω	=	Frequency, cps
[B]	=	Branch Transfer Matrix
[E]	=	Elasticity Transfer Matrix
[F]	=	Mass Transfer Matrix
[R]	=	Joint Transfer Matrix
$[\triangle]$	=	State Vector
AE	=	Beam Axial Stiffness Parameter $(\text{in}^2)(\text{lb}/\text{in}^2)$
BG	=	Torsional Stiffness Parameter, $(\text{in}^4)(\text{lb}/\text{in}^2)$
EI	=	Beam Stiffness Parameter, $(\text{lb}/\text{in}^2)(\text{in}^4)$

Subscripts

A	=	axial direction
L	=	left side of bay element
N	=	element number
R	=	right side of bay element
T	=	tangential direction

APPENDIX B

VIBRATION ANALYSIS USING

MATRIX TRANSFER METHODS

I.   VIBRATION ANALYSIS OF IN-PLANE LOADING OF IN-PLANE STRUCTURES
WITH BRANCHES

The general procedure of the matrix transfer method of analysis is outlined on pages B-5 through B-8 of this appendix. The detailed derivations and definitions of the elasticity, mass, and branch joint transfer matrices are also set forth.

The equations of equilibrium and compatibility for the elasticity element and lumped masses as well as the joint transfer equations for in-plane loading are as follows.

A.   ELASTICITY TRANSFER MATRIX
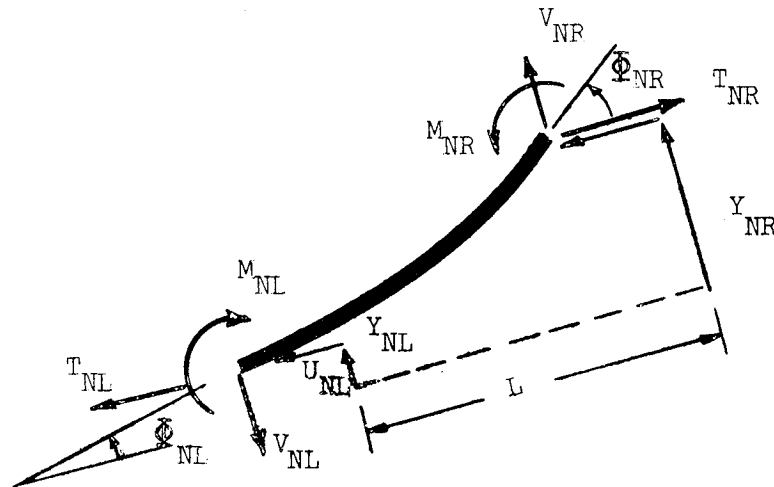
$$T_{NL} = T_{NR}; \quad V_{NL} = V_{NR}; \quad M_{NL} = M_{NR} + V_{NR} \cdot L$$

$$Y_{NL} = Y_{NR} - \Phi_{NR} \cdot L_N + \frac{M_{NR} \cdot L_N^2}{2 E I_N} + \frac{V_{NR} L_N^3}{6 E I_N} - \frac{V_{NR} \cdot c_N L_N}{G_N}$$

$$U_{NL} = U_{NR} + \frac{T_{NR} L_N}{(AE)_N}$$

$$\Phi_{NL} = \Phi_{NR} - \frac{M_{NR} L_N}{(EI)_N} - \frac{V_{NR} L_N^2}{2 (EI)_N}$$

In matrix form, the elasticity transfer matrix becomes:

$$
\begin{Bmatrix} T \\ V \\ M \\ Y \\ U \\ \Phi \end{Bmatrix}_{NR} =
\begin{bmatrix}
1 & 0 & 0 & 0 & 0 & 0 \\
0 & 1 & 0 & 0 & 0 & 0 \\
0 & L & 1 & 0 & 0 & 0 \\
0 & \left(\dfrac{L^3}{6EI} - \dfrac{CL}{Q}\right) & \dfrac{L^2}{2EI} & 1 & 0 & -L \\
\dfrac{L}{AE} & 0 & 0 & 0 & 1 & 0 \\
0 & \dfrac{-L^2}{2EI} & \dfrac{-L}{EI} & 0 & 0 & 1
\end{bmatrix}_N
\begin{Bmatrix} T \\ V \\ M \\ Y \\ U \\ \Phi \end{Bmatrix}_{NR}
$$

or $\quad \{\Delta\}_{NL} = [E]_N \{\Delta\}_{NR}$

B.　　MASS TRANSFER MATRIX
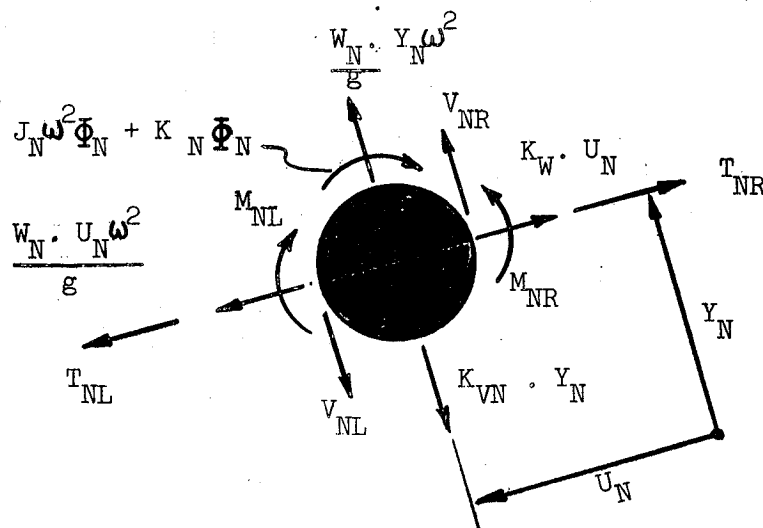
$$T_{NL} = T_{NR} + \left(K_T - \frac{Wn}{g}\,\omega^2\right) U_N$$

$$V_{NL} = V_{NR} + \left(-K_V + \frac{Wn}{g}\,\omega^2\right) Y_N$$

$$M_{NL} = M_{NR} - \left(K_\theta + J\,\omega^2\right) Y_N$$

$$U_{NL} = U_{NR}; \; \Phi_{NL} = \Phi_{NR}; \; Y_{NL} = Y_{NR}$$

In matrix form:

$$
\left\{ \begin{matrix} T \\ V \\ M \\ Y \\ U \\ \Phi \end{matrix} \right\}_{NL}
=
\begin{bmatrix}
1 & 0 & 0 & 0 & \left(K_T - \dfrac{W_N}{g}\,\omega^2\right) & 0 \\
0 & 1 & 0 & \left(-K_V + \dfrac{W_N}{g}\,\omega^2\right) & 0 & 0 \\
0 & 0 & 1 & 0 & 0 & -(K_\theta + J\omega^2) \\
0 & 0 & 0 & 1 & 0 & 0 \\
0 & 0 & 0 & 0 & 1 & 0 \\
0 & 0 & 0 & 0 & 0 & 1
\end{bmatrix}_N
\left\{ \begin{matrix} T \\ V \\ M \\ Y \\ U \\ \Phi \end{matrix} \right\}_{NR}
$$

or $\quad \{\Delta\}_{NL} = \begin{bmatrix} F \end{bmatrix}_N \{\Delta\}_{NR}$

C. JOINT TRANSFER MATRIX
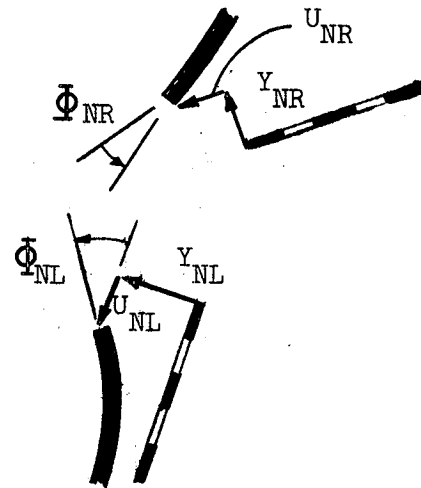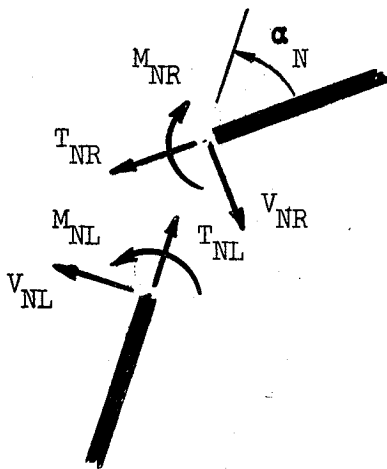
$$T_{NL} = T_{NR}\cos\alpha_N + V_{NR}\sin\alpha_N$$

$$V_{NL} = -T_{NR}\sin\alpha_N + V_{NR}\cos\alpha_N$$

$$M_{NL} = M_{NR}$$

$$Y_{NL} = Y_{NR}\cos\alpha_N + U_{NR}\sin\alpha_N$$

$$U_{NL} = -Y_{NR}\sin\alpha_N + U_{NR}\cos\alpha_N$$

$$\Phi_{NL} = \Phi_{NR}$$

In matrix form:

$$
\begin{Bmatrix} T \\ V \\ M \\ Y \\ U \\ \Phi \end{Bmatrix}_{NL}
=
\begin{bmatrix}
\cos\alpha & \sin\alpha & 0 & 0 & 0 & 0 \\
-\sin\alpha & \cos\alpha & 0 & 0 & 0 & 0 \\
0 & 0 & 1 & 0 & 0 & 0 \\
0 & 0 & 0 & \cos\alpha & \sin\alpha & 0 \\
0 & 0 & 0 & -\sin\alpha & \cos\alpha & 0 \\
0 & 0 & 0 & 0 & 0 & 1
\end{bmatrix}_{N}
\begin{Bmatrix} T \\ V \\ M \\ Y \\ U \\ \Phi \end{Bmatrix}_{NR}
$$

or $\{\Delta\}_{NL} = [R]_N \{\Delta\}_{NR}$

D.   BRANCH JOINT TRANSFER MATRIX
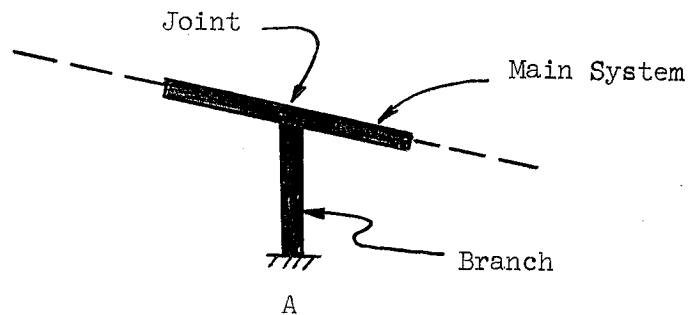
Starting at Point A "walking" to B with the aid of the transfer matrices we get

$$
\{\hat{\Delta}\}_B = \left[\prod_{N=1}^{N=\eta} \left([R]_N \; [E]_{NL} \; [F]_N \; [E]_{NR} \right) \right] \{\hat{\Delta}\}_A \qquad \textbf{Equation (1)}
$$

for η Bays in the branch.

Expanding Equation (1) gives:

$$
\{\,\hat{T}\ \ \hat{V}\ \ \hat{M}\ \ \hat{Y}\ \ \hat{U}\ \ \hat{\Phi}\ \ 1\,\}_B =
\begin{bmatrix}
d_{11} & d_{12} & d_{13} & d_{14} & d_{15} & d_{16} & d_{17}\\
 & & & & & & \\
 & & & & & & \\
 & & & & & & \\
 & & & & & & \\
d_{61} & d_{62} & d_{63} & d_{64} & d_{65} & d_{66} & d_{67}\\
0 & 0 & 0 & 0 & 0 & 0 & 1
\end{bmatrix}
\{\,T\ \ V\ \ M\ \ Y\ \ U\ \ \Phi\ \ 1\,\}_A = \{\,Q_1\ \ Q_2\ \ Q_3\ \ Q_4\ \ Q_5\ \ Q_6\ \ 1\,\}_B
$$

Equation (2)

Let $\hat{m},\ \hat{n},\ \hat{p}$ = Subscripts of unknowns at A.

$\hat{\xi},\ \hat{\eta},\ \hat{\beta}$ = Subscripts of given values at A.

Thus, rewriting Equation (2) gives

$$
\{\,\hat{T}\ \ \hat{V}\ \ \hat{M}\ \ \hat{Y}\ \ \hat{U}\ \ \hat{\Phi}\ \ 1\,\}_B =
\begin{bmatrix}
d_{1\hat{m}} & d_{1\hat{n}} & d_{1\hat{p}} & d_{1\hat{\xi}} & d_{1\hat{\eta}} & d_{1\hat{\beta}} & d_{17}\\
d_{2\hat{m}} & d_{2\hat{n}} & & & & & \\
 & & & & & & \\
 & & & & & & \\
 & & & & & & \\
d_{6\hat{m}} & & & & & d_{6\hat{\beta}} & d_{67}\\
0 & 0 & 0 & 0 & 0 & 0 & 1
\end{bmatrix}
\{\,Q_{\hat{m}}\ \ Q_{\hat{n}}\ \ Q_{\hat{p}}\ \ Q_{\hat{\xi}}\ \ Q_{\hat{\eta}}\ \ Q_{\hat{\beta}}\ \ 1\,\}_A
$$

Equation (3)

Now, writing Equation (3) in partitioned matrix form

$$
\{\,\hat{P}\ \mid\ \hat{W}\ \mid\ 1\,\}_B =
\left[
\begin{array}{cc|cc}
\xi_{11} & \xi_{12} & 17\\
\hline
\xi_{21} & \xi_{22} & 27\\
\hline
0 & 0 & 1
\end{array}
\right]
\{\,K_u\ \mid\ K_g\ \mid\ 1\,\}_A
$$

Equation (4)

Expanding Equation (4) gives

$$\hat{P} = \mathcal{E}_{11} \, K_u + \mathcal{E}_{12} \, K_g + d_{17} \qquad \text{Equation (5a)}$$

$$\hat{w} = \mathcal{E}_{21} \, K_u + \mathcal{E}_{22} \, K_g + d_{27} \qquad \text{Equation (5b)}$$

By multiplying Equation (5b) by $\mathcal{E}_{21}^{-1}$ we get

$$\mathcal{E}_{21}^{-1} \, \hat{w} = K_u + \mathcal{E}_{21}^{-1} \, \mathcal{E}_{22} \, K_g + \mathcal{E}_{21}^{-1} \cdot d_{27}$$

or

$$K_u = \mathcal{E}_{21}^{-1} \, \hat{w} - \mathcal{E}_{21}^{-1} \, \mathcal{E}_{22} \cdot K_g - \mathcal{E}_{21}^{-1} \cdot d_{27} \qquad \text{Equation (6)}$$

Substituting Equation (7) into Equation (6a) and writing in the partitioned

matrix form, we have:

$$\left\{ \begin{array}{c} \hat{P} \\ \hline 1 \end{array} \right\} = \left[\begin{array}{c|c|c} \mathcal{E}_{11} \, \mathcal{E}_{21}^{-1} & \mathcal{E}_{12} - \mathcal{E}_{11} \, \mathcal{E}_{21}^{-1} \, \mathcal{E}_{22} & d_{17} - \mathcal{E}_{11} \, \mathcal{E}_{21}^{-1} \, d_{27} \\ \hline 0 & 0 & 1 \end{array} \right] \left\{ \begin{array}{c} \hat{w} \\ K_g \\ \hline 1 \end{array} \right\} \quad \begin{array}{c} \text{Equation} \\ \text{(7)} \end{array}$$

Expanding Equation (7) gives

$$\left\{ \begin{array}{c} \hat{T} \\ \hat{V} \\ \hat{M} \\ \hline 1 \end{array} \right\}_B = \left[\begin{array}{ccc|ccc|c} \hat{k}_{11} & \hat{k}_{12} & \hat{k}_{13} & \hat{k}_{14} & \hat{k}_{15} & \hat{k}_{16} & \hat{k}_{17} \\ \hat{k}_{21} & \hat{k}_{22} & \hat{k}_{23} & \hat{k}_{24} & \hat{k}_{25} & \hat{k}_{26} & \hat{k}_{18} \\ \hat{k}_{31} & \hat{k}_{32} & \hat{k}_{33} & \hat{k}_{34} & \hat{k}_{35} & \hat{k}_{36} & \hat{k}_{19} \\ \hline 0 & 0 & 0 & 0 & 0 & 0 & 1 \end{array} \right] \left\{ \begin{array}{c} \hat{Y}_B \\ \hat{U}_B \\ \hat{\Phi}_B \\ \hline Q\hat{\xi} \\ Q\hat{\eta} \\ Q\hat{\beta} \\ \hline 1 \end{array} \right\} \quad \text{Equation (7a)}$$

Hence, we now have the forces at Point B in terms of the displacements at B
and the known boundary conditions at Point A. However, these values are with
respect to the sign convention of the branch; therefore, a change of coordinates
transfer matric is needed. For simplicity, rewriting Equation (7) and
Equation (7a) as

$$
\left\{ \begin{array}{c} \widehat{P}_A \\ \hline 1 \end{array} \right\}
\left[\begin{array}{ccc} K_{11} & K_{12} & K_{13} \\ 0 & 0 & 1 \end{array} \right]
\left\{ \begin{array}{c} W_B \\ \hline K_g \\ \hline 1 \end{array} \right\}
\qquad \text{Equation (8)}
$$

and multiplying by the appropriate coordinate transfer matrix $\begin{bmatrix} G_1 \end{bmatrix}$ yields

$$
\left\{ \begin{array}{c} P_B \\ \hline 1 \end{array} \right\} =
\left[\begin{array}{ccc|c}
G_1 \mathcal{E}_{11} \mathcal{E}_{21}{}^{-1} G_1{}^{-1} & G_1 \mathcal{E}_{12} - G_1 \mathcal{E}_{11} \mathcal{E}_{21}{}^{-1} \mathcal{E}_{22} & G_1 d_{12} - G_1 \mathcal{E}_{11} \mathcal{E}_{21}{}^{-1} d_{27} \\
\hline 0 & 0 & 1
\end{array} \right]
\left\{ \begin{array}{c} \widehat{w}_B \\ \hline K_g \\ \hline 1 \end{array} \right\}
\quad \text{Equation (9)}
$$

where:
$$
G_1 = G_2 = \left[\begin{array}{ccc}
\cos \Upsilon & \sin \Upsilon & 0 \\
-\sin \Upsilon & \cos \Upsilon & 0 \\
0 & 0 & 1
\end{array} \right]
$$

Expanding Equation (9) we have imposed on the main system from the branch

$$
\left\{
\begin{array}{c}
T_B \\
V_B \\
M_B \\
1
\end{array}
\right\}
=
\left[
\begin{array}{ccccccc}
k_{11} & k_{12} & k_{13} & k_{14} & k_{15} & k_{16} & k_{17} \\
k_{21} & k_{22} & k_{23} & k_{24} & k_{25} & k_{26} & k_{27} \\
k_{31} & k_{32} & k_{33} & k_{34} & k_{35} & k_{36} & k_{37} \\
0 & 0 & 0 & 0 & 0 & 0 & 1
\end{array}
\right]
\left\{
\begin{array}{c}
Y_B \\
U_B \\
\Phi_B \\
Q_{\hat{\xi}} \\
Q_{\hat{\eta}} \\
Q_{\hat{\beta}} \\
1
\end{array}
\right\}
\qquad \text{Equation (10)}
$$

We are now ready to write down the branch joint transfer matrix. Consider the joint point of the main system.
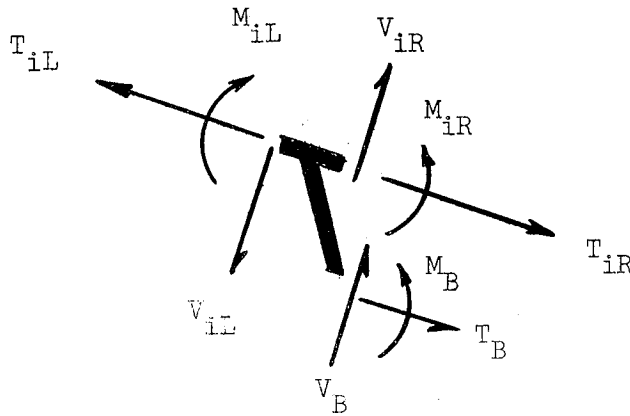
The equilibrium equations are:

$$
V_{iL} = V_{iR} + V_B; \quad T_{iL} = T_{iR} + T_B; \quad M_{iL} = M_{iR} + M_B \qquad \text{Equation (11)}
$$

The branch joint transfer matrix is:

$$
\begin{Bmatrix} T \\ V \\ M \\ Y \\ U \\ \Theta \\ 1 \end{Bmatrix}_{iL}
=
\begin{bmatrix}
1 & 0 & 0 & k_{11} & k_{12} & k_{13} & k_{14}Q_{\xi}+k_{15}Q_{\eta}+k_{16}Q_{\beta}+k_{17} \\
0 & 1 & 0 & k_{21} & k_{22} & k_{23} & k_{24}Q_{\xi}+k_{25}Q_{\eta}+k_{26}Q_{\beta}+k_{27} \\
0 & 0 & 1 & k_{31} & k_{32} & k_{33} & k_{34}Q_{\xi}+k_{35}Q_{\eta}+k_{36}Q_{\beta}+k_{37} \\
0 & 0 & 0 & 1 & 0 & 0 & 0 \\
0 & 0 & 0 & 0 & 1 & 0 & 0 \\
0 & 0 & 0 & 0 & 0 & 1 & 0 \\
0 & 0 & 0 & 0 & 0 & 0 & 1
\end{bmatrix}
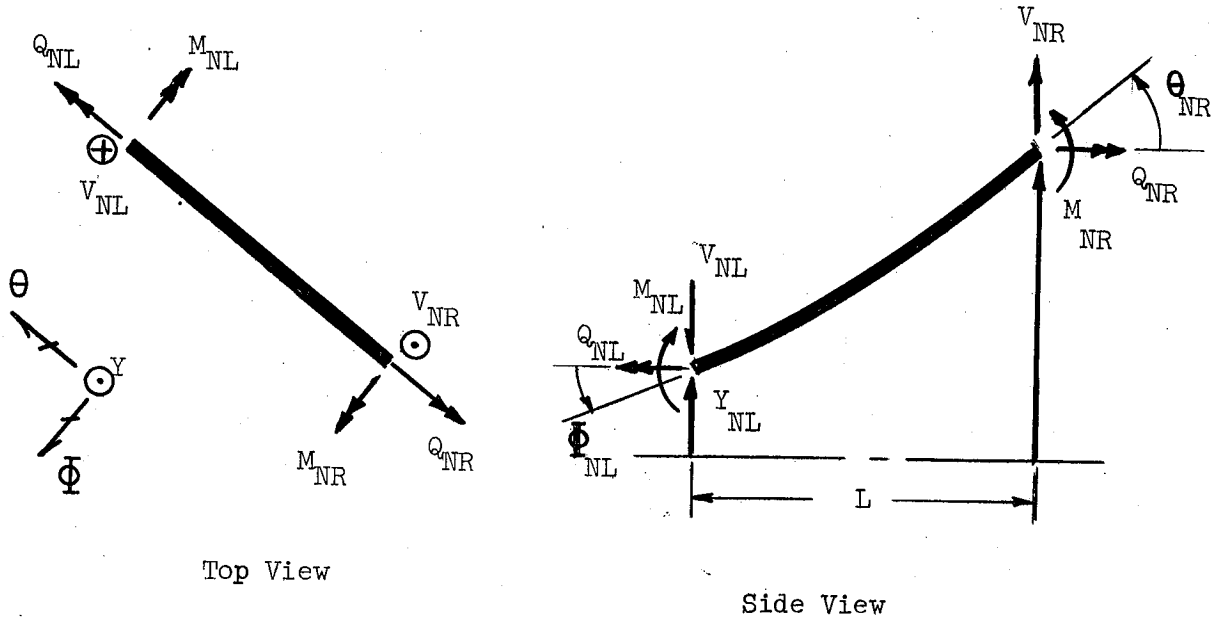\begin{Bmatrix} T \\ V \\ M \\ Y \\ U \\ \Theta \\ 1 \end{Bmatrix}_{iR}
$$

or

$$\{\Delta\}_{iL} = [B]_i \{\Delta\}_{iR}$$

II. VIBRATION ANALYSIS OF OUT-OF-PHASE LOADING OF IN-PLANE STRUCTURES WITH BRANCHES

The equations of equilibrium and compatibility for the elasticity element and lumped masses and the joint transfer equations for out-of-plane loading are as follows.

A. ELASTICITY TRANSFER MATRIX

Top View

Side View

$$V_{NL} = V_{NR}$$

$$M_{NL} = M_{NR} + V_{NR} \cdot L$$

$$Q_{NL} = Q_{NR}$$

$$Y_{NL} = Y_{NR} - \Phi_{NR} \cdot L + \frac{M_{NR} L^2}{2EI} + \left(\frac{L^3}{6EI} - \frac{CL}{G} \right) V_{NR}$$

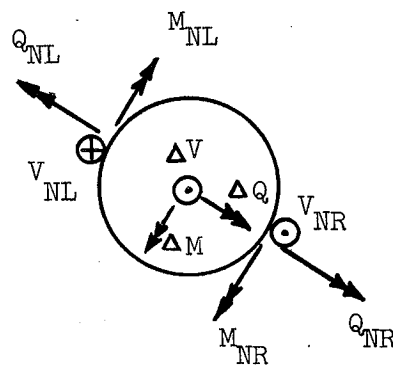$$\Phi_{NL} = \Phi_{NR} - \frac{M_{NR}}{EI} - \frac{V_{NR} L^2}{2EI}$$

$$\theta_{NL} = \theta_{NR} + \frac{Q_{NR} L}{BG}$$

In Matrix Form:

$$
\left\{
\begin{array}{c}
V \\
M \\
Q \\
Y \\
\Phi \\
\theta
\end{array}
\right\}_{NL}
=
\begin{bmatrix}
1 & 0 & 0 & 0 & 0 & 0 \\
L & 1 & 0 & 0 & 0 & 0 \\
0 & 0 & 1 & 0 & 0 & 0 \\
(\frac{L^3}{6EI} - \frac{CL}{G}) & \frac{L^2}{2EI} & 0 & 1 & -L & 0 \\
\frac{-L^2}{2EI} & -\frac{I}{EI} & 0 & 0 & 1 & 0 \\
0 & 0 & \frac{L}{BG} & 0 & 0 & 1
\end{bmatrix}_{N}
\left\{
\begin{array}{c}
V \\
M \\
Q \\
Y \\
\Phi \\
\theta
\end{array}
\right\}_{NR}
$$

$$\text{or } \{\Delta\}_{NL} = [E]_N \{\Delta\}_{NR}$$

B.   **MASS TRANSFER MATRIX**

Top View

Side View

$$V_{NL} = V_{NR} + \frac{W_n}{g}\,\bar{V}\,\omega^2 + \bar{V} - K_\theta\,\theta_N - K_Y\,Y_N$$

$$M_{NL} = M_{NR} - K_M\,\Phi_N + \bar{M}$$

$$Q_{NL} = Q_{NR} + (J\omega^2 - K_T)\,\theta_N + \bar{Q}$$

$$\Delta Q \doteq (J\omega^2 - K_T)\,\theta_N$$

$$Y_{NL} = Y_{NR} \quad ; \quad \theta_{NL} = \theta_N + \bar{Q} \quad ; \quad \Phi_{NL} = \Phi_{NR}$$

In Matrix form:

$$
\begin{Bmatrix} V \\ M \\ Q \\ Y \\ \Phi \\ \theta \\ 1 \end{Bmatrix}_{NL}
=
\begin{bmatrix}
1 & 0 & 0 & 0 & 0 & \left(\frac{W_n}{g}\omega^2 - K\,\theta_N\right) & 0 \\
0 & 1 & 0 & 0 & -K_M & 0 & 0 \\
0 & 0 & 1 & 0 & 0 & (J\omega^2 - K_T) & 0 \\
0 & 0 & 0 & 1 & 0 & 0 & 0 \\
0 & 0 & 0 & 0 & 1 & 0 & 0 \\
0 & 0 & 0 & 0 & 0 & 1 & 0 \\
0 & 0 & 0 & 0 & 0 & 0 & 1
\end{bmatrix}
\cdot
\begin{Bmatrix} V \\ M \\ Q \\ Y \\ \Phi \\ \theta \\ 1 \end{Bmatrix}_{NR}
$$

or $\{\Delta\}_{NL} = [F]_N \{\Delta\}_{NR}$

C. JOINT TRANSFER MATRIX
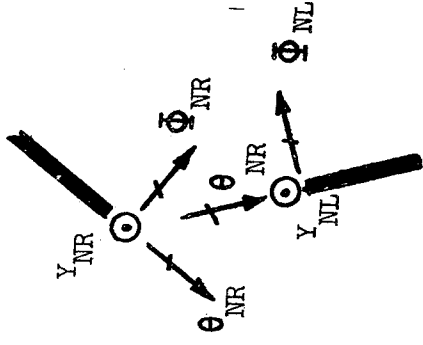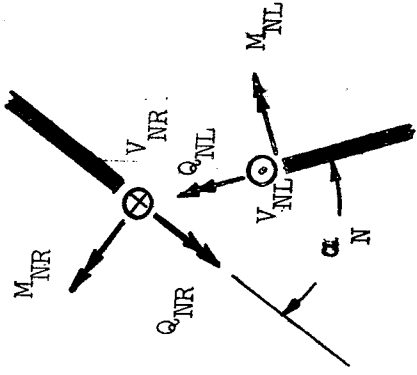
$V_{NL} = V_{NR}$; $Y_{NL} = Y_{NR}$

$M_{NL} = Q_{NR} \sin\alpha_N + M_{NR} \cos\alpha_N$

$Q_{NL} = Q_{NR} \cos\alpha_N + M_{NR} \sin\alpha_N$

$\Phi_{NL} = \Phi_{NR} \cos\alpha_N - \Phi_{NR} \sin\alpha_N$

$\theta_{NL} = \theta_{NR} \sin\alpha_N - \theta_{NR} \cos\alpha_N$

In Matrix Form:

$$
\begin{Bmatrix} V \\ M \\ Q \\ Y \\ \Phi \\ \theta \end{Bmatrix}_{NL}
=
\begin{bmatrix}
1 & 0 & 0 & 0 & 0 & 0 \\
0 & \cos\alpha_N & \sin\alpha_N & 0 & 0 & 0 \\
0 & \sin\alpha_N & \cos\alpha_N & 0 & 0 & 0 \\
0 & 0 & 0 & 1 & 0 & 0 \\
0 & 0 & 0 & 0 & \cos\alpha_N & -\sin\alpha_N \\
0 & 0 & 0 & 0 & \sin\alpha_N & -\cos\alpha_N
\end{bmatrix}_N
\begin{Bmatrix} V \\ M \\ Q \\ Y \\ \Phi \\ \theta \end{Bmatrix}_{NR}
$$

D.   BRANCH JOINT TRANSFER MATRIX

The branch joint transfer matrix equations for out-of-plane loading are derived in the same manner as for the in-plane loading; therefore, refer to section I, D, page B-4.

W. F. Dankhoff (3 Copies)
National Aeronautics and Space Administration
Lewis Research Center
21000 Brookpark Road
Cleveland, Ohio   44135
Mail Stop 500-305

H. Hinckley (1 Copy)
Mail Stop 500-310

Patent Counsel (1 Copy)
Mail Stop 77-1

Lewis Library (2 Copies)
Mail Stop 60-3

M. J. Hartmann (1 Copy)
Mail Stop 5-9

W. L. Stewart (1 Copy)
Mail Stop 5-9

J. C. Montgomery (1 Copy)
SNPO-C
Mail Stop 501-1

Major E. H. Karalis (1 Copy)
AFSC Liaison Office
Mail Stop 4-1

Office of Reliability and Quality
   Assurance (1 Copy)
Mail Stop 500-203

F. J. Dutee (1 Copy)
Mail Stop 23-1

D. F. Lange (1 Copy)
Mail Stop 501-1

J. B. Esgar (1 Copy)
Mail Stop 49-1

D. D. Scheer (1 Copy)
Mail Stop 500-305

G. F. Zalabak (1 Copy)
Mail Stop 500-305

NASA Headquarters (6 Copies)
NASA Scientific and Technical
   Information Facility
Box 5700
Bethesda, Maryland

Library (1 Copy)
NASA
Ames Research Center
Moffett Field, California   94035

Library (1 Copy)
NASA
Flight Research Center
P. O. Box 273
Edwards AFB, California   93523

Library (1 Copy)
NASA
Langley Research Center
Langley Station
Hampton, Virginia   23365

Library (1 Copy)
NASA
Manned Spacecraft Center
Houston, Texas   77058

Library (1 Copy)
NASA
Goddard Space Flight Center
Greenbelt, Maryland   20771

Library (1 Copy)
NASA
George C. Marshall Space Flight Center
Huntsville, Alabama   35812

Library (1 Copy)
NASA
Western Operations Office
150 Pico Boulevard
Santa Monica, California   90406

Library (1 Copy)
Jet Propulsion Laboratory
4800 Oak Grove Drive
Pasadena, California   91103

A. O. Tischler (2 Copies)
NASA Headquarters
Code RP
Washington, D. C.   20546

J. W. Thomas, Jr. (5 Copies)
NASA   I-E-E
George C. Marshall Space Flight Center
Huntsville, Alabama   35812

E. W. Gomersall (1 Copy)
NASA
Mission Analysis Division
Office of Advanced Research and Technology
Moffett Field, California   94035

Dr. K. Boyer (1 Copy)
Los Alamos Scientific Laboratory
CMF-9
P. O. Box 1663
Los Alamos, New Mexico

A. Schmidt (1 Copy)
National Bureau of Standards
Cryogenic Division
Boulder, Colorado

Dr. C. Wislicenus (1 Copy)
Penn State University
Naval Ordinance Laboratory
University Park, Pennsylvania

Dr. A. Acosta (1 Copy)
California Institute of Technology
1201 East California Street
Pasadena, California

Dr. E. B. Konecci (1 Copy)
National Aeronautics and Space Administration
Executive Office of the President
Executive Office Building
Washington, D. C.

Dr. M. Vavra (1 Copy)
Naval Post Graduate School
Monterey, California

H. V. Main (1 Copy)
Air Force Rocket Propulsion Laboratory
Edwards Air Force Base
Edwards, California

Dr. G. Serovy (1 Copy)
Iowa State University
Ames, Iowa

T. Iura (1 Copy)
Aerospace Corporation
2400 East El Segundo Boulevard
P. O. Box 95085
Los Angeles, California   90045

Chemical Propulsion Information Agency (1 Copy)
Johns Hopkins University
Applied Physics Laboratory
8621 Georgia Avenue
Silver Springs, Maryland

R. O. Bullock (1 Copy)
Garrett Corporation
Airesearch Manufacturing Division
402 S. 36th Street
Phoenix, Arizona   85034

Pratt and Whitney Aircraft Corporation (1 Copy)
Florida Research and Development Center
P. O. Box 2691
West Palm Beach, Florida   33402

Library Department 586-306 (1 Copy)
Rocketdyne, Division of North American Aviation
6633 Canoga Avenue
Canoga Park, California   91304

J. Stanitz (1 Copy)
Thompson-Ramo-Wooldridge, Inc.
23444 Euclid Avenue
Cleveland, Ohio   44117

Dr. M. J. Zucrow (1 Copy)
Purdue University
Lafayette, Indiana   47907